Energy Conversion and Management 325 (2025) 119338

Contents lists available at ScienceDirect

Energy Conversion and Management

journal homepage: www.elsevier.com/locate/enconman

Research paper

Optimizing temperature and pressure in PEM electrolyzers: A model-based approach to enhanced efficiency in integrated energy systems

Luka Bornemann *, Jelto Lange, Martin Kaltschmitt

Institute of Environmental Technology and Energy Economics, Hamburg University of Technology, Eissendorfer Strasse 40, 21073 Hamburg, Germany

ARTICLE INFO

Dataset link: https://doi.org/10.5281/zenodo.13269351, Code and Data for Paper: Optimizing Temperature and Pressure in PEM Electrolyzers: A Model-Based Approach to Enhanced Efficiency in Integrated Energy Systems (Original data)

Keywords:
Green hydrogen
Polymer-electrolyte-membrane electrolyzer
Energy system optimization
Process optimization
Nonlinear programming

ABSTRACT

Hydrogen stands as a promising energy carrier within the ongoing energy supply transformation, yet its production via electrolyzers remains prohibitively costly. To address this challenge, this paper proposes an advanced equation-oriented process model for a PEM (Polymer-Electrolyte-Membrane) electrolysis system, including the electrolyzer and downstream hydrogen compression, aimed at optimizing the interaction of its operating parameters (i.e., current density, temperature, pressure). Initially, the model is utilized to analyze the isolated performance of the electrolysis system through operational flowsheet optimizations, followed by its integration into a broader energy system for operational planning optimization.

The study reveals several key findings: optimizing operational parameters, rather than using fixed values at the maximum, improves peak system efficiency by approximately 5 %pt. and shifts this peak to lower current densities, thus expanding the range of high-efficiency operation. Each current density has an optimal pair of temperature and pressure, with maximum temperatures only advantageous at loads above 40%, while maximum operating pressure is suboptimal across the entire load range. The analysis indicates that incorporating operating parameter optimization within the operational planning of the electrolysis system reduces energy consumption by 4% and operating costs by 7% in the evaluated energy system.

Additionally, the study distinguishes between optimizing the electrolyzer's operating parameters for maximizing its own efficiency and for system efficiency (i.e., including hydrogen compression). It demonstrates that maximum system efficiency is achievable only when the electrolyzer considers hydrogen compression in its operation mode, accepting some efficiency losses individually but yielding greater efficiency gains in the context of hydrogen compression.

In summary, the findings of this paper suggest that continuously operating a PEM electrolyzer at maximum temperature and pressure may not be the most efficient approach. Instead, dynamic adjustments based on current density improve operational efficiency, thereby reducing electricity consumption and operating costs. Evaluating the electrolyzer within the broader energy system context – and accepting minor efficiency losses at the electrolyzer level – can yield significant overall benefits and savings. These results underscore the importance of comprehensive, context-aware strategies in advancing cost-effective green hydrogen production.

1. Introduction

Hydrogen has the potential to play a pivotal role in the transition from fossil fuel-based to renewable energy systems, offering a crucial solution for combating climate change [1]. By using electricity from renewable energies, electrolyzers can produce hydrogen and oxygen by splitting of water and, thus, enable bulk storage of potentially intermittent renewable energy [2]. Thema et al. [3] forecast that the worldwide installed capacity of electrolyzers could increase up to 100 000 MW in the year 2050, underlining the future relevance of electrolyzers. Polymer-electrolyte-membrane (PEM) electrolyzers in particular are able to dynamically adapt their operation to the prevailing conditions (e.g., supply of renewable energies [4], grid serviceability [5], and electricity prices [6]). This adaptability makes them well-suited for integration into future renewable energy systems [7]. However, additional reductions in costs and enhancements in energy efficiency are necessary for electrolyzers to achieve commercial viability in hydrogen-based energy systems [8].

Apart from ongoing technical advancements and economy of scale effects [9], cost reduction can be achieved through optimization of the electrolyzer's operating mode. Firstly, the operation of a specific electrolyzer can be scheduled to maximize hydrogen production during favorable conditions within the overarching energy system (e.g., low

* Corresponding author.
E-mail address: luka.bornemann@tuhh.de (L. Bornemann).

https://doi.org/10.1016/j.enconman.2024.119338
Received 9 August 2024; Received in revised form 6 November 2024; Accepted 27 November 2024

Nomenclature

Latin letters

A	Active cell area [m^2]
a	Activity [–]
C	Operating costs [€]
c	Energy price [€/kWh]
$\boldsymbol{d}$	Decision variables [–]
d	Thickness [m]
$\dot{E}$	Generalized power [MW]
E	Capacity [MW(h)]
E_A	Activation energy [J/mol]
F	Faraday constant [C/mol]
f	Fugacity [bar]
$\boldsymbol{g}$	Inequality constraints [–]
G	Gibbs energy [kJ/mol]
$\boldsymbol{h}$	Equality constraints [–]
H	Enthalpy [kJ/mol]
I	Current [A]
j	Current density [A/cm^2]
j_0	Current exchange density [A/cm^2]
$\dot{n}$	Molar flow [mol/s]
n	Number [–]
P	Power [kW]
p	Pressure [bar]
$\dot{Q}$	Heat [kW]
R	Gas constant [J/mol/K]
R_0	Interface resistance [Ω/cm^2]
T	Temperature [K]
t	Time step [h]
U	Voltage [V]
z	Number electrons [–]

Greek letters

α	Charge transfer coefficient [–]
Δ	Difference [–]
δ	Swelling factor [–]
η	Efficiency [–]
σ	Resistance [–]
Y	Proportionality constant [bar cm^2/A]

Sets

$\mathcal{D}$	Set of all decision variables
$\mathcal{E}$	Set of all energy carriers
$\mathcal{J}$	Set of all operating points
$\mathcal{T}$	Set of all time steps

Superscripts

buy	Buying
charge	Charging
D	Demand
diff	Diffusion
discharge	Discharging
gas	Gaseous
H2S	Hydrogen storage
in	Input
max	Maximum
min	Minimum
N	Nominal
out	Output
PV	Photovoltaics
reac	Reaction
rel	Relative
sell	Selling
tot	Total
vap	Vapor

Subscripts

a	Anode
act	Activation
c	Cathode
cell	Cell
comp	Compression
e	Energy carrier
el	Electricity
ev	Evaporation
faraday	Faraday
H_2	Hydrogen
H_2O	Water
heat	Heating
k	Component
l	Liquid
mech	Mechanical
min	Minimal
m	Membrane
O_2	Oxygen
ocv	Open-circuit
o	Operating point
preheat	Pre-heating
ratio	Ratio
ref	Reference
res	Resistance
Stack	Stack
stages	Compression stages
System	System
tb	Thermobalanced
tn	Thermoneutral
t	Time step
use	Usage
voltage	Voltage
waste	Waste heat

Abbreviations

AHC	Anodic hydrogen content
LHV	Lower heating value
LP	Linear programming
NLP	Nonlinear programming
SOC	State of charge

electricity prices [6], surplus renewable energy [4]). Secondly, adjusting the operating parameters of electrolyzers can enhance operational efficiency, decrease electricity consumption, and consequently reduce operating costs [10,11].

In terms of operation, three parameters primarily affect the operational efficiency of electrolyzers: the load point, operating temperature, and operating pressure [2]. The impacts of these three parameters on operational efficiency have been thoroughly examined in the past [2]. While a maximum efficiency tends to occur at lower load points [12],

the optimal temperature and pressure settings are less clear. Electrolyzer manufacturers are increasingly permitting higher temperatures [13] and pressures [14]. In theory, higher temperatures offer thermodynamic benefits, leading to reduced overvoltage and improved efficiency [15]. Likewise, since it is advantageous to store hydrogen at high pressure levels, higher pressures within the electrolyzer minimize subsequent mechanical compression, thereby conserving compression energy and enhancing overall efficiency [16]. Therefore, it seems advantageous to operate at the highest possible pressure and temperature levels whenever feasible.

However, investigations that consider the electrolyzer not just at the cell level but as an entire system, including balance of plant components and compression, show that this conclusion is not necessarily accurate. Analytical studies on a PEM electrolyzer, factoring in downstream mechanical compression, have revealed that each load point possesses its unique optimum operating pressure, which may not coincide with the maximum permissible pressure [17,18]. Similarly, the same principle applies to temperature. Studies have indicated that lower temperatures are optimal at lower loads, while at higher loads, the temperature aligns with the maximum permitted temperature [13, 19]. When determining the operation of an electrolyzer, it is therefore crucial to consider the following points to ensure optimal operating efficiency:

- Taking a comprehensive perspective of the overall electrolyzer system, encompassing its entire operation up to the utilization of hydrogen (e.g., including subsequent compression), rather than solely focusing on the cell.
- Considering the simultaneous adjustment of pressure, temperature, and load point.

The studies referenced above rely on analytical models, primarily employed for static analysis of individual operating points of stand-alone electrolyzers, lacking integration for time-variant operation within an energy system. Consequently, these models do not facilitate a quantitative assessment of the effects and advantages, such as energy or cost savings, arising from adjusting operating parameters in the integrated operation of an electrolyzer within an energy system.

This approach necessitates enhanced models. Energy system optimization models are conventionally employed to explore operational strategies of energy systems. When using models to optimize energy systems, typically a compromise has to be made between the complexity of the model and the computing time [20]. In operational optimization of electrolyzers, the impact of the load point on operational efficiency has been adequately reflected in numerous studies, ensuring computational efficiency [21,22]. However, since the description of operating parameters such as pressure and temperature often introduce nonlinear correlations [23], these are usually neglected or modeled in a simplified manner. For example, two approaches regarding temperature are identified in literature.

- The first considers temperature's impact on operational efficiency, but ties it to the load point, thus restricting independent selection regardless of the load point [24–26].
- The second approach enables independent temperature selection using cooling capacity; however, so far, this has only been applied to stand-alone electrolyzers, without exploring integrated operation within an energy system [10].

Furthermore, Valverde et al. [27] considered the impact of operating pressure on operational efficiency, yet they treated it as a fixed parameter, without allowing for any variable adjustment. Prokopou et al. [28] developed a process model for a PEM-based electrochemical hydrogen compressor, enabling dynamic optimization of the pressure and temperature. However, since this model only considers electrochemical compression, it neglects important properties of a PEM electrolyzer. Thus, there is a lack of electrolyzer models that enable the independent optimization of pressure, temperature, and load point within an operational optimization framework. This capability is crucial for fully realizing the potential for enhancing operational efficiency through the variable adjustment of operating parameters within a hydrogen-based energy system's operational optimization.

Contribution of this work. To address this gap, this paper proposes an equation-oriented process model for a PEM electrolysis system (i.e., PEM electrolyzer including downstream compression), aiming to optimize the operational efficiency of such an electrolysis system within the respective energy system. The proposed process model incorporates the thermophysical and technical properties of a PEM electrolyzer, providing a detailed modeling of its operating behavior. The equation-oriented approach allows for the description of the reaction properties based on the enthalpies and Gibbs energies of material mixtures and the calculation of phase equilibria, thereby eliminating the need for frequently used empirical relationships. Simultaneously, it enables both stand-alone analysis as part of operational flowsheet optimization and integrative analysis as part of operational energy system optimization. This dual capability provides comprehensive insights into optimizing operational efficiency by variably adjusting the operating parameters of a PEM electrolyzer.

To this end, the PEM electrolysis system model is first analyzed as an isolated unit under static conditions. Through operational flowsheet optimizations, the optimal operating pressure and temperature for maximizing efficiency are determined for selected load points, thus obtaining characteristics for the entire operating range. Efficiency is examined in two modes: one where the electrolyzer accounts for compression in its operation and another where it optimizes its own operation independently. The process model presented here thus provides new insights into optimal operating parameters for electrolysis systems. Specifically, this approach reveals the extent to which optimal operating parameters differ when (1) the electrolyzer aims to maximize its own efficiency, and (2) when it incorporates downstream hydrogen compression, thereby striving to maximize the overall system efficiency.

Subsequently, the process model is integrated into an energy system model. The impact of optimizing operating efficiency on energy consumption and operating costs is investigated through integrated operational planning, utilizing time-variable adjustments of the operating parameters. Unlike existing literature, this approach allows for the variation of operating parameters to determine optimal strategies for the electrolyzer system within the framework of an energy system. This potential for energy and cost savings is highlighted, enabling conclusions to be drawn regarding the real-world operation of electrolyzers for more cost-efficient green hydrogen production.

In summary, this paper aims to provide a comprehensive assessment of the potential savings achievable through the optimization of operating parameters in a PEM electrolyzer, along with the required implementations.

To achieve these goals, the paper is structured as follows: Section 2 describes the methodological approach, including the presentation of the process model of the PEM electrolysis system and the procedure for determining the operating range characteristics, as well as the presentation of the energy system and the associated optimization problem formulation. Section 3 presents and discusses the results, followed by the conclusion outlined in Section 4.

2. Methodological approach

Fig. 1 outlines the general structure and methodological approach of this work, which can be divided into two main parts:

- Part A (Section 2.1) introduces the process model of a PEM electrolysis system, including a stand-alone PEM electrolyzer and subsequent downstream compression. Here, the developed process model is initially applied as an isolated unit. Through operational

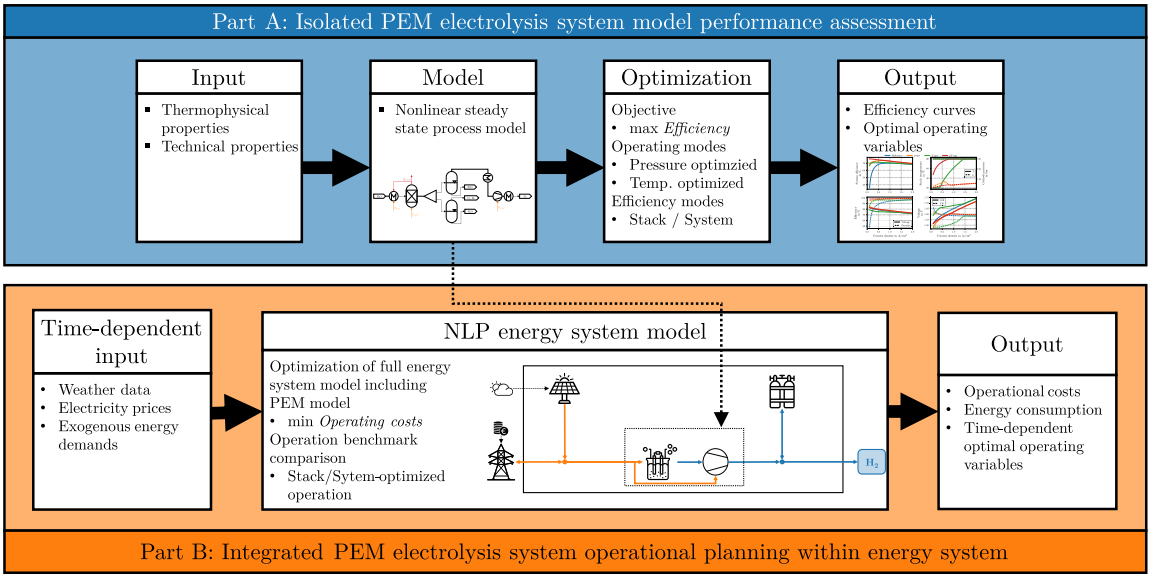

Fig. 1. Overview of the methodology used in this paper.
Source: Adapted from Wiegner et al. [29].

flowsheet optimizations, the optimal operating pressure and temperature for maximizing efficiency are determined for selected load points under static conditions. This approach yields the operating characteristics in the form of efficiency and operating parameter curves across the entire load range.

- In Part B (Section 2.2), the time-variable selection of the optimal operating parameters and their influence on energy consumption and operating costs are investigated as part of operational planning. For this purpose, the process model is integrated into an overarching PV-hydrogen energy system model, and an operational energy system optimization is carried out based on the given input time series.

The following sections discuss these two parts in more detail.

2.1. Part A: Isolated PEM electrolysis system model performance assessment

The process model of a PEM electrolysis system, including a standalone PEM electrolyzer and downstream compression, is presented below. In this paper, the term 'electrolysis system' refers to the electrolyzer along with the subsequent compression. When only the term 'electrolyzer' is used, it pertains solely to the system boundary of the electrolyzer up to, but not including, the compression stage.

The process model of the electrolysis system is developed using the IDAES Integrated Platform [30]. This Python framework provides predefined unit models (e.g., heat exchangers, reactors) that can be interconnected to create a flowsheet optimization model.

The general workflow of the IDAES Integrated Platform begins with modeling the operation of each unit, specifying material properties (e.g., thermophysical properties of pure substances) and reaction properties (e.g., reaction equations, conversion rates), as well as the operating behavior of the unit (e.g., isothermal operation of a reactor). The units are then linked to define the material flow and the overall flowsheet (Section 2.1.1). Finally, additional overarching (in)equality constraints (e.g., concentration limits, efficiencies) (Section 2.1.2) and objective functions (e.g., operating costs) are incorporated for optimization (Section 2.1.3).

2.1.1. Flowsheet

The following describes the process of creating the flowsheet of the PEM electrolysis system using the integrated IDAES platform by presenting the predefined unit models utilized and their interconnections. A process flowsheet is a schematic representation of the complete process, including material and energy flows. It defines the process units involved (e.g., heat exchangers, reactors) and their interconnections, which in turn specify the material (e.g., water, hydrogen) and energy flows (e.g., electricity, heat) [31]. Consequently, a flowsheet can be used to visualize the process flow and, in the context of modeling, provide insights into the submodels employed and how they are utilized to represent specific process characteristics.

The flowsheet of the PEM electrolysis system is shown in Fig. 2. The electrolysis system considered in this work consists of two main parts: the stack and the compression section. Within the stack, process water is first preheated to the desired stack temperature T_{stack} in a heat exchanger. If the internally generated waste heat $\dot{Q}_{waste}$ is insufficient for this purpose, it is typically supplemented with electrical heating elements [19]; i.e., the external required heat is supplied by electrical power P_{heat}. The electrolysis reaction then takes place in the cell reactor (stoichiometric reactor) with an additional supply of electricity $U_{cell}I$. Since isothermal operation of the reactor is assumed, the excess waste heat generated $\dot{Q}_{waste}$ is released into the environment. A membrane separator unit is used to split the reaction products into hydrogen (cathode) and oxygen (anode) streams. Phase equilibrium is established, and liquid water is separated in the respective flash units.

The anode side operates at atmospheric pressure, while the cathode pressure p_{cat} can be freely selected as an optimization variable. Due to diffusion processes, minor amounts of the hydrogen and oxygen produced permeate through the membrane to the anode and cathode, respectively [32]. It is assumed that oxygen and hydrogen at the cathode recombine to form water [12], resulting in a mixture of hydrogen and water vapor leaving the cathode. No recombination occurs at the anode [33]; i.e., hydrogen and oxygen are present simultaneously, making the anodic hydrogen content (AHC) an important safety parameter [34].

Outside the stack, the hydrogen flow undergoes a compression process to guarantee the final pressure p_{use} of 200 bar using a 5-stage isentropic compression (compressor unit), with intermediate cooling to 40 °C [18] in a heat exchanger. This pressure level corresponds to a typically realized pressure level for on-site storage in industry [35] and the storage pressure in salt caverns [36], thus covering a wide range of applications. Only the required electrical power for compression P_{comp} is considered, without accounting for the waste heat generated during the compression process; this waste heat is assumed to be a loss.

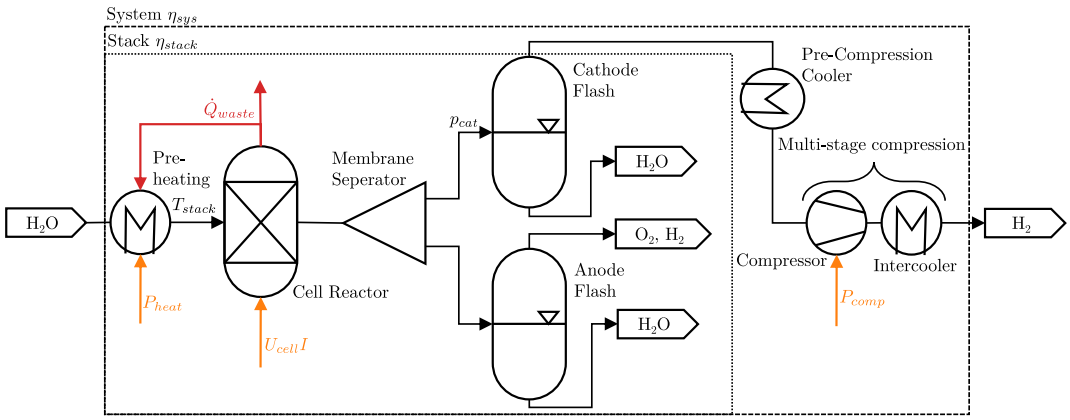

Fig. 2. Visualization of the flowsheet of the PEM electrolysis system.

2.1.2. Electrochemical model

Since the electrochemical correlations and processes within an electrolyzer cell are not predefined in the IDAES platform, they must be added manually. This electrochemical submodel, which facilitates the calculation and optimization of the PEM electrolysis system's efficiency (see Fig. 2), is detailed in this subsection. The submodel incorporates both fundamental thermodynamic equations and experimental correlations, linking technical parameters (e.g., membrane thickness, membrane permeability) with thermophysical parameters (e.g., material properties of hydrogen). It is, therefore, a mathematical representation of an electrolyzer, without considering the real technical constraints of implementation.

The efficiency is primarily influenced by factors such as cell voltage, heat management, gas crossover, and subsequent compression. These factors are briefly explained below to facilitate an understanding of the final results. A more detailed overview for reproducing the results can be found in Appendix A.1.

Stack and system efficiency. In the electrolysis system under consideration, water is split into hydrogen and oxygen with the addition of electrical power P_{el}; the provided hydrogen is then further compressed within a downstream compression process. The most general way to represent the efficiency η is by the ratio of the supplied electrical power to the energy content of the hydrogen outlet flow (Eq. (1)). The energy content of the hydrogen results from the molar flow $\dot{n}_{H_2}$ in relation to the lower calorific value LHV_{H_2}.

$$\eta = \frac{\dot{n}_{H_2} LHV_{H_2}}{P_{el}} \tag{1}$$

The electrical power is required to chemically split the water molecule. The respective electrical power is defined by the applied cell voltage U_{cell} and the resulting current flow I. Additionally, an external heat supply might be needed to maintain a constant stack temperature, assumed to be provided by an electric heating element via the heat supply P_{heat}. Finally, the compression power P_{comp} is needed to compress the hydrogen.

In this paper, a distinction is made between stack efficiency η_{stack} (Eq. (2)) and system efficiency η_{sys} (Eq. (3)). Unlike system efficiency, stack efficiency does not account for the electrical power required for the subsequent compression of the hydrogen.

$$\eta_{stack} = \frac{\dot{n}_{H_2} LHV_{H_2}}{U_{cell} I + P_{heat}} \tag{2}$$

$$\eta_{sys} = \frac{\dot{n}_{H_2} LHV_{H_2}}{U_{cell} I + P_{heat} + P_{comp}} \tag{3}$$

Cell voltage. The cell voltage U_{cell} must be applied to the electrolysis cell for the electrolysis reaction (i.e., splitting of water into hydrogen and oxygen) to occur. Under ideal, reversible conditions, the cell voltage corresponds to the open-circuit voltage U_{ocv}. However, once the electrolysis reaction begins and current flows, the necessary cell voltage increases due to irreversibilities (i.e., overvoltages). In this work, activation overvoltages arising from kinetic limitations, and ohmic overvoltages resulting from the ohmic resistances within the cell, are taken into account. Diffusion overvoltages are not considered, as they are negligibly small at the current densities examined in this study (see Table 1) [37]. Therefore, the cell voltage consists of the open-circuit voltage U_{ocv}, the activation overvoltage U_{act}, and the ohmic overvoltage U_{res} (Eq. (4) [38]).

$$U_{cell} = U_{ocv} + U_{act} + U_{res} \tag{4}$$

The voltage efficiency $\eta_{voltage}$ can be defined as a measure of the cell voltage U_{cell}, relating the actual cell voltage to the ideal, reversible open-circuit voltage U_{ocv} (Eq. (5)).

$$\eta_{voltage} = \frac{U_{ocv}}{U_{cell}} \tag{5}$$

Heat management. During the electrolysis reaction, two opposing processes occur in the cell that influence heat management.

- Heat is generated by the ohmic overvoltages and activation overvoltages heating up the electrolyzer cell.
- The phase change from liquid water to gaseous hydrogen and oxygen, as well as the vaporization of water, requires enthalpy of vaporization, which cools the cell.

In addition, heat must be used to preheat the process water to the desired stack temperature [12]. These relationships are expressed via the thermobalanced voltage U_{tb} (Eq. (6) [12]). This depends on factors such as the thermoneutral voltage U_{tn}, water preheating $\dot{Q}_{heat}$, the evaporation energy of the water vapor H_{ev}^{gas}, and the Faraday constant F.

$$U_{tb} = U_{tn} + \frac{\dot{Q}_{heat}}{2F} + \frac{H_{ev}^{gas}}{2F} \tag{6}$$

If the cell voltage U_{cell} corresponds to the thermobalanced voltage U_{tb}, the heat balance of the cell is equalized. When the applied cell voltage exceeds the thermobalanced voltage, waste heat $\dot{Q}_{waste}$ is generated. Conversely, if the applied cell voltage falls below the thermobalanced voltage, external heating P_{heat} of the cell is required (Eq. (7) [12]).

$$\begin{aligned} \dot{Q}_{waste} &= (U_{cell} - U_{tb})I, \quad \text{for } U_{cell} > U_{tb} \\ P_{heat} &= (U_{tb} - U_{cell})I, \quad \text{for } U_{cell} < U_{tb} \end{aligned} \tag{7}$$

Gas crossover. The PEM electrolyzer considered here uses a polymer electrolyte membrane, typically made of Nafion [39]. The primary function of the membrane is to ensure proton conductivity while separating oxygen at the anode from hydrogen at the cathode.

However, there is still some permeation of the two gases through the membrane [32]. The permeated oxygen recombines with the hydrogen already produced at the cathode, resulting in a loss of usable

hydrogen [12]. Similarly, the permeated hydrogen leads directly to a loss of usable hydrogen. Unlike at the cathode, this hydrogen does not react with the oxygen at the anode but remains in parallel [33]. The proportion of hydrogen in the gas mixture at the anode is quantified by the anodic hydrogen content (AHC). If the AHC exceeds a threshold of 4%, a potentially explosive mixture is formed, which must be avoided [34].

According to Fick's law, the diffusion of oxygen and hydrogen $\dot{n}_i^{diff}$ can be expressed as a function of the temperature-dependent permeability of the membrane ϵ_i, the fugacity difference between the anode and cathode Δf_i, the membrane thickness $d_m\delta_m$, and the active cell area A (Eq. (8) [28]).

$$\dot{n}_i^{diff} = \epsilon_i(T)\, A \frac{\Delta f_i}{d_m \delta_m}, \quad \forall i \in \{H_2, O_2\} \tag{8}$$

Additionally, for hydrogen at the cathode and oxygen at the anode, the increase in partial pressure p_i^* due to gas evolution must be taken into account. This is achieved using a proportionality factor Y dependent on the current density j, for the partial pressure of hydrogen at the cathode $p^c_{H_2}$ and the partial pressure of oxygen at the anode $p^a_{O_2}$, as illustrated in Schalenbach et al. [12] (Eq. (9)).

$$\begin{aligned} p^{c,*}_{H_2} &= p^c_{H_2} + Y j \\ p^{a,*}_{O_2} &= p^a_{O_2} + Y j \end{aligned} \tag{9}$$

The final usable material flow of hydrogen $\dot{n}_{H_2}$ is calculated as the difference between the total hydrogen produced $\dot{n}^{tot}_{H_2}$ and the diffusion losses (Eq. (10)).

$$\dot{n}_{H_2} = \dot{n}^{tot}_{H_2} - \dot{n}^{diff}_{H_2} - 2\dot{n}^{diff}_{O_2} \tag{10}$$

The Faraday efficiency $\eta_{faraday}$ can be defined as a measure of the gas crossover, relating the usable material flow of hydrogen $\dot{n}_{H_2}$ to the total hydrogen produced $\dot{n}^{tot}_{H_2}$ (Eq. (11)).

$$\eta_{faraday} = \frac{\dot{n}_{H_2}}{\dot{n}^{tot}_{H_2}} \tag{11}$$

Compression. Here, a multi-stage compression to a working pressure p_{use} of 200 bar is assumed [35,36]. When compressing hydrogen, the temperature should not exceed 140 °C between compression stages. To achieve this, a compression ratio p_{ratio} of approximately 2.6 or less per stage must be maintained [18].

Preliminary investigations regarding the minimum output pressure of the electrolyzer have shown that 5 compression stages n_{stages} are necessary for the model under consideration and the application case, as determined by Eq. (12).

$$n_{stages} \geq \frac{\log\left(\frac{p_{use}}{p_{min}}\right)}{\log p_{ratio}} \tag{12}$$

In the process model, compression is modeled as a single-stage isentropic compression including pre- and post-cooling. The total compression power P_{comp} is, thus, the result of the single-stage compression power P^1_{comp} multiplied by the number of compression stages n_{stages} (Eq. (13)).

$$P_{comp} = n_{stages} P^1_{comp} \tag{13}$$

A validation of the implemented electrochemical model can be found in Figs. B.1 to B.3.

2.1.3. Optimization problem

The aim of Part A is to generate data that describes the optimal operation of the stand-alone electrolysis system. To achieve this, a flowsheet optimization model is created based on the flowsheet, including the electrochemical submodel. The PEM electrolysis system aims to reduce energy consumption and operating costs by maximizing efficiency. In this context, two efficiency modes are defined:

- *System-optimized.* The electrolyzer has access to information from the downstream compression and can adjust its operating mode accordingly during hydrogen production aiming to maximize system efficiency.
- *Stack-optimized.* The electrolyzer does not have access to compression information and can only maximize its own operational efficiency, thus maximizing stack efficiency.

To maximize efficiency, the electrolyzer can adjust the operating parameters of stack temperature and cathode pressure (i.e., the pressure of the hydrogen at the output of the electrolyzer). Four operating modes (see Table 1) are defined for this purpose:

- Reference mode. The operating parameters are not adjusted. A fixed stack temperature of 80 °C and a fixed cathode pressure of 30 bar are assumed, representing a state-of-the-art PEM electrolyzer [2].
- *p*-opt mode. The stack temperature remains fixed at 80 °C, but the cathode pressure is freely selectable.
- *T*-opt mode. The cathode pressure is fixed at 30 bar, but the stack temperature is freely selectable.
- *pT*-opt mode. Both the stack temperature and the cathode pressure are freely selectable, allowing for a high degree of flexibility.

Table 1
Overview of the operating modes and choice of operating parameters. The selectable current density j corresponds to 0.1 A/cm² to 2 A/cm² for all modes.

Operating mode	T_{stack}	p_{cat}
Reference	80 °C	30 bar
p-opt	80 °C	1 bar to 30 bar
T-opt	20 °C to 80 °C	30 bar
pT-opt	20 °C to 80 °C	1 bar to 30 bar

These different operating modes enable the investigation of the influence of each operating parameter on the efficiency of the electrolysis system. Based on the efficiency and operating modes, an optimization problem following the formulation from Wang et al. [21] is defined in Eq. (14).

Depending on the efficiency mode, either the stack efficiency η_{stack} or the system efficiency η_{sys} is maximized as the objective (Eq. (14a)). Eqs. (14b) and (14c) summarize all constraints of the previously described flowsheet model (e.g., electrochemical equations, material balances, energy balances). The free decision variables are summarized in the vector $\boldsymbol{d}$. Depending on the operating mode, this vector includes either the stack temperature, the cathode pressure, or both. In the reference mode, there are no free decision variables, resulting in a fully determined optimization problem with no degrees of freedom.

The implementation of the IDAES platform includes further variables (e.g., enthalpies, molar fractions), but these are dependent on the free decision variables and thus do not represent degrees of freedom in the optimization problem. Therefore, these variables are not listed.

To obtain information on the operating behavior across the entire operating range, the optimization problem is solved for a selection of operating points o (Eq. (14d)). An operating point is defined by the choice of current density j, which is fixed at a specific value j_o within the permissible range for each optimization run $(j_o \in \mathcal{J})$. A minimum current density of 0.1 A/cm² and a maximum current density of 2 A/cm² are selected as state-of-the-art parameters [2].

$$\max_{\boldsymbol{d}} \quad \eta_{stack}(\boldsymbol{d}), \eta_{sys}(\boldsymbol{d}) \tag{14a}$$

$$\text{s.t.} \quad \boldsymbol{h}(\boldsymbol{d}) = \boldsymbol{0} \tag{14b}$$

$$\boldsymbol{g}(\boldsymbol{d}) \leq \boldsymbol{0} \tag{14c}$$

$$j = j_o \qquad j_o \in \mathcal{J} \subset [0.1, 2]\,\text{A/cm}^2 \tag{14d}$$

$$\boldsymbol{d} \in \mathcal{D} = \{T_{stack}, p_{cat}\} \tag{14e}$$

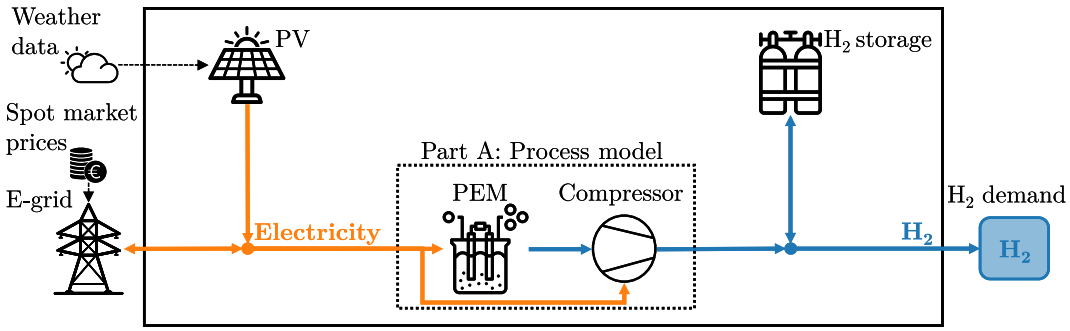

Fig. 3. Energy system structure (E: Electricity, PV: Photovoltaic system, PEM: Polymer electrolyte membrane electrolyzer).

The resulting nonlinear programming (NLP) optimization problem is solved using the open-source solver IPOPT [40], yielding a local optimum. To ensure reliable and reproducible results, it is essential to initialize each variable with stable and consistent starting values, especially when solving NLP optimization problems. For calculating the efficiency at the first optimized operating point, the automated initialization functions of the IDAES platform are used; for all subsequent operating points, the results from the previous operating point serve as starting values. This approach ensures consistency within each operating mode across the entire load range. Additionally, to maintain consistency across different operating modes, the same initialization values are applied for the first optimized point of each operating mode.

2.2. Part B: Integrated electrolysis system operational planning within energy system

After investigating the behavior of the isolated PEM electrolysis system for static operating points in Part A (Section 2.1), now the optimal time-variable operating parameters of the PEM electrolysis system are investigated within the context of operational planning in an energy system, interacting with other energy system components. To achieve this, the PEM electrolysis system process model is integrated into a PV-hydrogen energy system model, and an operational energy system optimization is conducted. This is done for the operating modes 'Reference' and 'pT-opt' regarding the two efficiency modes 'Stack-optimized' and 'System-optimized'. The goal is to demonstrate how the choice of operating parameters in time-variant operation differs between the cases and how this choice affects energy consumption and operating costs.

Section 2.2.1 and Section 2.2.2 first describe the structure of the energy system and the time-dependent input data. The optimization problem underlying the operational planning is then presented in Section 2.2.3.

2.2.1. Energy system structure

In addition to the PEM electrolysis system, the energy system under consideration also includes a hydrogen storage system and a PV system (see Fig. 3). The aim of this overall energy system is to meet an externally defined hydrogen demand. The hydrogen is produced and compressed within the PEM electrolysis system and can either be used directly to satisfy the hydrogen demand or temporarily stored in the hydrogen storage.

The electricity required for the PEM electrolysis system is supplied either by the PV system or the power grid. Surplus electricity generated by the PV system can also be fed back into the grid, enabling a bi-directional flow of electricity.

2.2.2. Input data

Time-dependent weather data and electricity price data are stored as time series in the energy system model (Fig. 4) to investigate the operation of the PEM electrolysis system under time-varying boundary conditions. The weather data is assumed to correspond to a site near Hamburg, Germany and has already been converted into the relative output power of the PV system [41]. The electricity prices are divided into purchase and sales prices.

- The sales price reflects the electricity market prices in Germany for the year 2023 [42].
- The purchase price is based on the sales price, with additional taxes, fees, and charges applicable to non-household customers in the year 2023 [43].

Due to the high computational effort caused by the non-linearities of the PEM electrolysis system process model, the time series for the entire year are aggregated into 7 typical days of 24 h each using a time series aggregation. This aggregation is performed using the hierarchical clustering method [44,45] (via tool tsam [46]).

Table 2
Nominal capacity E_k^N of the energy system components based on Sens et al. [47].

Component k	E_k^N
PEM electrolysis system	1 MW
PV system	2.5 MW
Hydrogen storage	49.3 MWh

The dimensioning of the components (see Table 2) is based on a location-dependent cost-optimized PV-hydrogen energy system Sens et al. [47]. This approach ensures that the sizing and composition of the energy system components are grounded in a comprehensive economic analysis to guarantee minimum-cost hydrogen production. Consequently, the energy system under consideration is representative of future cost-effective, hydrogen-based energy systems, making the results of this work broadly applicable. For the integration of the PEM electrolysis model, it is assumed that all electrolyzer cells operate identically and that the rated power of the electrolyzer is defined by the active cell area (see Table A.1). In this setup, a current density of 2 A/cm^2 corresponds to a load of 1 MW. However, the PEM electrolysis model can be scaled as needed for additional case studies. The exogenous hydrogen demand is set to ensure that the PEM electrolysis system achieves a cost-optimal annual full-load hour figure of approximately 4500 h [47]. Additionally, it is assumed that this hydrogen will be used to supply an industrial operation or a similar application that requires a continuous hydrogen supply, resulting in a fixed hourly hydrogen demand of around 513 kWh.

2.2.3. Optimization problem

The optimal operational planning of the energy system is represented through an operational optimization problem using the formulation by Wang et al. [21] in Eq. (15).

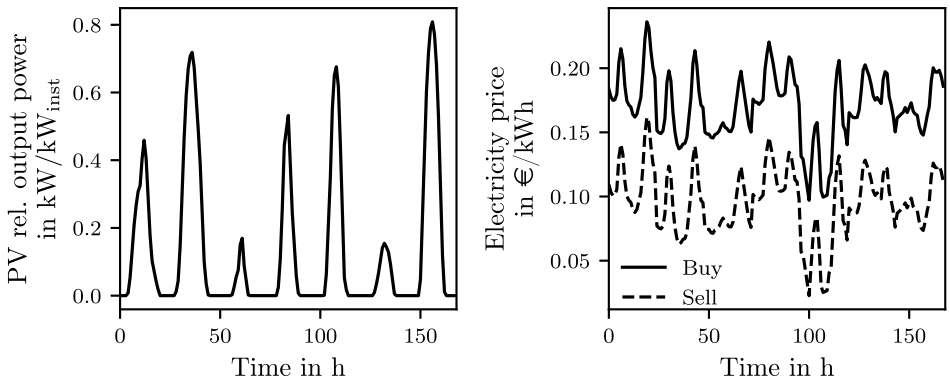

Fig. 4. Presentation of the time series input data of the relative PV output power and electricity prices. The values shown are based on a time series aggregation with 7 typical days and 24 time steps of 1 h in each case.

The aim of the optimization is to minimize the operating costs C resulting from the purchase and sale of electricity within the energy system (Eq. (15a)). The parameter $c_{el,t}^{buy/sell}$ represents the electricity purchase or sales price, and $\dot{E}_{el,t}^{buy/sell}$ denotes the amount of energy purchased or fed into the electrical grid. Simultaneously, the required external energy demand $\dot{E}_{e,t}^{D}$ must be covered at any time step ($\forall t \in \mathcal{T}$), and the energy balances must be equalized (Eq. (15b)). The components of the energy system (i.e., PEM electrolysis system, PV system, and hydrogen storage system) are collectively referred to as the set $\mathcal{K}$. Each component has an input and output $\dot{E}_{k,e,t}^{in/out}$ flow related to the energy carrier $e \in \mathcal{E}$ (i.e., hydrogen, electricity).

The input and output flows of the PEM electrolysis system are integrated into the energy system model via Eqs. (15c) and (15d). The output flow $\dot{E}_{PEM,H_2,t}^{out}$ pertains to the energy content of the usable hydrogen, while the input flow $\dot{E}_{PEM,el,t}^{in}$ corresponds to the electricity requirement for the production and compression of hydrogen. As stated in the isolated PEM electrolysis system flowsheet optimization (Eq. (14)), the stack temperature $T_{stack,t}$ and/or the cathode pressure $p_{cat,t}$ are free optimization variables, depending on the operating mode. Due to the dynamic nature of operational planning, the current density j_t for each operating mode is also a free optimization variable to enable variable hydrogen production over time.

Additionally, the input and output flows of the other energy system components are included in the vector $\dot{\boldsymbol{E}}$, and these are also free optimization variables in the operational planning. All other constraints originating from both the energy system model and the process model are summarized in Eq. (15e).

$$\min_{\boldsymbol{d},\dot{\boldsymbol{E}}} \quad C = \sum_{t\in\mathcal{T}} \Delta t \left(c_{el,t}^{buy} \dot{E}_{el,t}^{buy} - c_{el,t}^{sell} \dot{E}_{el,t}^{sell} \right) \tag{15a}$$

$$\text{s.t.} \quad \sum_{k\in\mathcal{K}} \left(\dot{E}_{k,e,t}^{out} - \dot{E}_{k,e,t}^{in} \right) + \dot{E}_{e,t}^{buy} - \dot{E}_{e,t}^{sell} = \dot{E}_{e,t}^{D}, \tag{15b}$$

$$\forall e \in \mathcal{E}, \forall t \in \mathcal{T}$$

$$\dot{E}_{PEM,H_2,t}^{out} = \dot{n}_{H_2,t} LHV_{H_2}, \qquad \forall t \in \mathcal{T} \tag{15c}$$

$$\dot{E}_{PEM,el,t}^{in} = U_{cell,t} I_t + P_{heat,t} + P_{comp,t}, \tag{15d}$$

$$\forall t \in \mathcal{T}$$

$$\boldsymbol{g}\left(\boldsymbol{d}, \dot{\boldsymbol{E}}\right) \leq \boldsymbol{0}, \qquad \forall k \in \mathcal{K}, \forall e \in \mathcal{E}, \forall t \in \mathcal{T} \tag{15e}$$

$$\boldsymbol{d} \in D = \left\{ T_{stack,t}, p_{cat,t}, j_t \right\},$$

$$\dot{\boldsymbol{E}} \in \left\{ \dot{E}_{k,e,t}^{out}, \dot{E}_{k,e,t}^{in}, \dot{E}_{el,t}^{buy}, \dot{E}_{el,t}^{sell} \right\} \tag{15f}$$

The modeling of the other energy system components is detailed in Appendix A.2. The formulation by Kotzur et al. [48] is employed for modeling the hydrogen storage to facilitate storage across days despite the aggregated and non-chronological time series.

The energy system optimization model is implemented using the Python optimization framework Pyomo [49,50]. Apart from the electrolysis system process model, the remaining component models are formulated as linear programming (LP) optimization models (see Appendix A.2). The integration of the NLP electrolysis system process model results in an NLP optimization problem for the energy system. Analogous to Section 2.1.3, the energy system optimization problem is solved using the solver IPOPT [40]. For integrated operation, the PEM electrolysis system model is initialized at each time step with the starting values corresponding to the operating point of 1 A/cm^2. This initialization approach is applied across all operating modes to ensure consistency.

3. Results and discussion

The results derived from applying the methodology are presented and discussed below. This presentation follows the methodology and will first show the findings for the isolated electrolysis system model performance assessment in Section 3.1, followed by the results for its integrated operation within the energy system under consideration in Section 3.2.

3.1. Part A: Isolated electrolysis system model performance assessment

The isolated operation of the electrolysis system is analyzed below. Since system efficiency optimization is the primary objective, the operating characteristics for this case are presented first. Subsequently, an analysis of the differences between the system-optimized and stack-optimized cases is carried out.

3.1.1. Optimal operating characteristics

Fig. 5 illustrates the curves of the optimal operating parameters across the entire operating range for system efficiency optimization. The operating modes 'Reference', 'p-opt', 'T-opt', and 'pT-opt' are considered. The diagram presents the system efficiency, stack temperature and cathode pressure, voltage and Faraday efficiency, and cell and thermobalanced voltages. Unless otherwise stated, all following comparisons refer to the 'Reference' case.

System efficiency. Below the results related to the system efficiency are discussed in detail.

- The temperature optimization (T-opt) shifts the point of maximum system efficiency towards lower current densities by steadily decreasing the temperature below a current density of 1.5 A/cm^2 until the minimum temperature of 20 °C is reached at a current density of around 0.4 A/cm^2.
- The pressure optimization (p-opt) generally raises the efficiency curve, enabling a higher maximum system efficiency, but this maximum is reached already at a current density of around 0.6 A/cm^2. Coming from low current densities, the pressure rises steadily from around 2 bar to a local maximum of around 7 bar at 0.6 A/cm^2, then drops slightly and then rises again to around 6 bar at 2 A/cm^2.

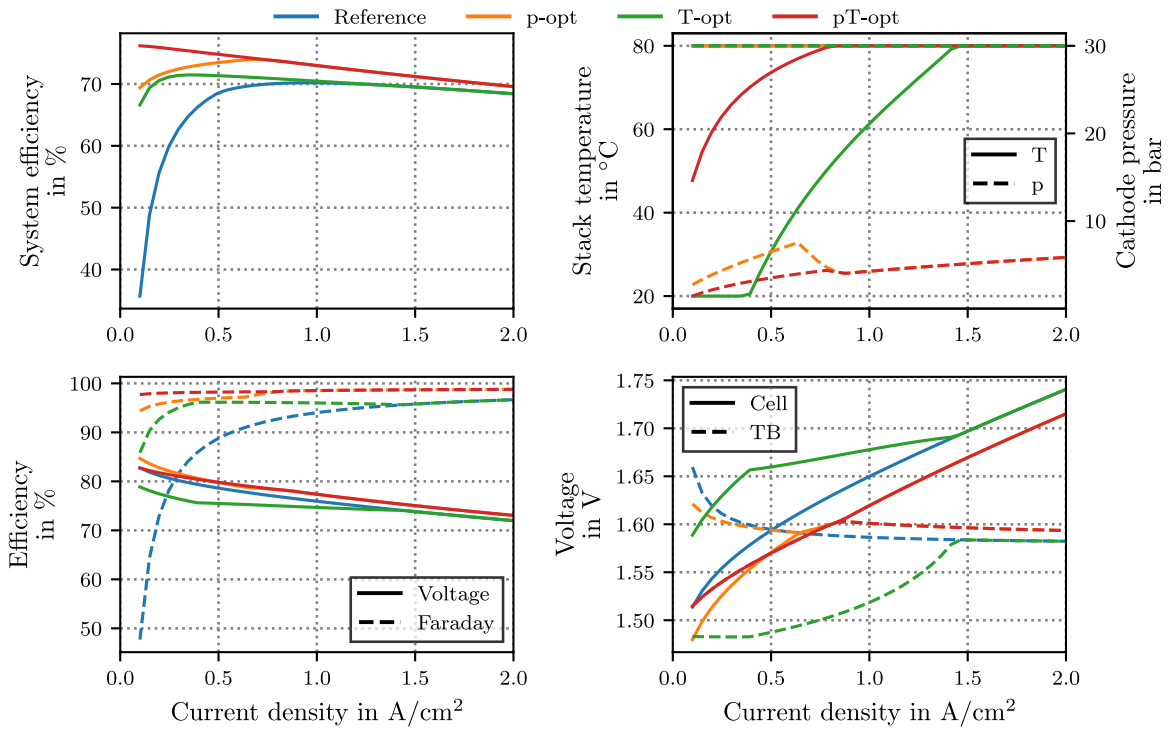

Fig. 5. Optimal operating parameters and efficiencies (depicted by hatching) for the various operating modes (depicted by color). The aim of the optimization is to maximize system efficiency η_{sys}, including compression to 200 bar (system-optimized) (TB: Thermobalanced).

- The simultaneous pressure and temperature optimization (pT-opt) combines both of these advantages. At high current densities, the same pressure is chosen as in pressure optimization (p-opt), whereby the same increase in efficiency is achieved. At lower current densities, a lower pressure is selected compared to pressure optimization (p-opt) and the drop in temperature occurs at lower temperatures compared to temperature optimization (T-opt). Both phenomena ensure that a drop in system efficiency is avoided at low current densities and thus the maximum is reached at the minimum permitted current density of 0.1 A/cm^2.

Temperature. The temperature-optimized (T-opt) case illustrates the rationale for adjusting the temperature. When the current density drops below 1.5 A/cm^2, both the voltage efficiency and the Faraday efficiency deviate from the reference case. Although the voltage efficiency slightly decreases, the significant drop in Faraday efficiency is prevented, thereby maintaining a higher system efficiency. However, once the minimum stack temperature is reached at a current density of around 0.4 A/cm^2, both the Faraday efficiency and, consequently, the system efficiency decline. At low current densities, the gas crossover mechanism dominates and can be mitigated by uniformly reducing the stack temperature (Eqs. (8) and (A.12)).

Heat management. Coming from high current densities, between a current density of 0.6 A/cm^2 and 0.8 A/cm^2, the p-opt and pT-opt cases exhibit a complex mechanism. Above a current density of 0.8 A/cm^2, the cell voltage exceeds the thermobalanced voltage in both the p-opt and pT-opt cases. This eliminates the need for external heating (Eq. (7)), and system efficiency optimization only involves balancing the cell voltage against the compression needs (Eq. (3)). However, at a current density of 0.8 A/cm^2, the cell voltage and thermobalanced voltage intersect, necessitating the consideration of external heating for system efficiency optimization.

In both the p-opt and pT-opt cases, efforts are made to avoid external heating by ensuring that the cell voltage remains above the thermobalanced voltage (Eq. (A.7)), thus maintaining thermal balance.

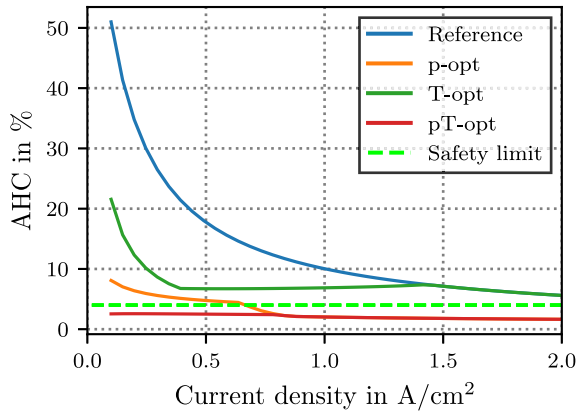

Fig. 6. Anodic hydrogen content (AHC) for the various operating modes regarding the optimization of the system efficiency η_{sys}, including compression to 200 bar (system-optimized).

In the p-opt case, pressure is initially increased down to a current density of 0.6 A/cm^2 to maintain thermal balance. However, below 0.6 A/cm^2, further pressure increases would result in significant gas crossover losses, necessitating a pressure reduction and acceptance of external heating to maintain system efficiency.

In the pT-opt case, coming from high current densities, the pressure is also increased (local maximum) and then reduced to mitigate gas crossover losses, albeit at a lower level. Additionally, by lowering the temperature, the thermobalanced voltage can be aligned with the cell voltage, thereby balancing the thermal requirements without necessitating external heating. The curve of the influencing parameters on the thermobalanced voltage for the respective cases is shown in Fig. C.1.

Gas crossover. The Faraday efficiency and the anodic hydrogen content (AHC) serve as a measure of the gas crossover. A drop in Faraday efficiency can be observed at low current densities in all cases. This in

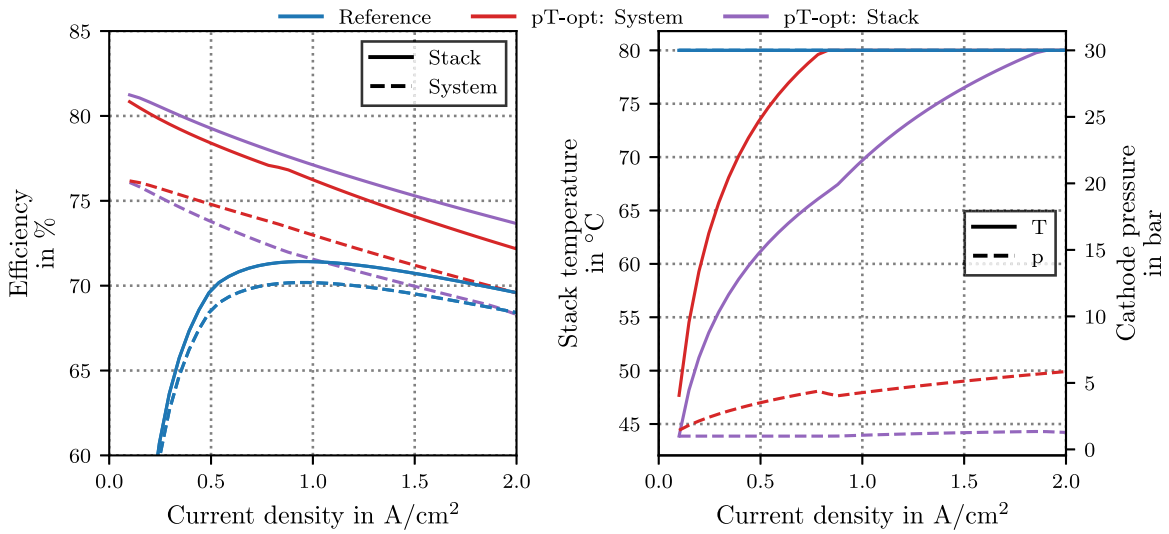

Fig. 7. Comparison of stack and system efficiency and choice of operating parameters (depicted by hatching) for different current densities when either stack efficiency (purple) or system efficiency (red) including downstream compression is optimized. Only the simultaneous pressure and temperature optimized case (*pT*-opt) and the reference case are illustrated.

turn is reflected in an increase in the anodic hydrogen content (Fig. 6). As the gas crossover increases with increasing pressure and temperature (Eqs. (A.11) and (A.12)), the reference case has the highest anodic hydrogen content. By lowering the temperature (*T*-opt) and pressure (*p*-opt), the increase in anodic hydrogen content can be delayed and the overall level lowered. Nevertheless, the three cases exceed the permissible limit value partially (*p*-opt) or completely (reference, *T*-opt). Exceeding the limit value can only be prevented by simultaneously adjusting the pressure and temperature (*pT*-opt). Additional safety measures (e.g., catalyst materials) are necessary to ensure safety-uncritical operation, particularly in the reference and *T*-opt cases.

3.1.2. Comparison of stack- and system-optimized operation

In Fig. 7, the investigation focuses on how the choice of operating parameters changes when optimizing for stack efficiency alone versus system efficiency, which includes compression. Stack-optimized operation represents the most efficient mode that a stand-alone electrolyzer can achieve. This scenario applies either when no additional information about subsequent compression is available for planning the electrolyzer's operation or when the focus is solely on optimizing the stand-alone operation of the electrolyzer.

Pressure. Compared to system efficiency optimization, atmospheric pressure is selected for current densities below $1\,A/cm^2$. At higher current densities, the pressure increases slightly, but is still far below compared to the system efficiency optimization case. Increased pressure results in higher gas crossover (Eq. (A.11)) and open-circuit voltage (Eq. (A.2)), thereby providing no advantage at the stack level.

Temperature. Lower temperatures are selected for stack efficiency optimization so that the maximum permissible temperature of 80 °C is only reached near nominal current densities. Throughout the entire load range, a similar effect regarding heat management is observed here as in the system-optimized case for low current densities (Fig. 5). Opting for low pressure results in a higher concentration of water vapor in the product gases due to phase equilibrium, consequently leading to an elevated thermobalanced voltage. In stack-optimized operation, the temperature is adjusted across the entire operating range to align the cell voltage with the thermobalanced voltage, thereby eliminating the need for heating the electrolyzer or generating waste heat (Fig. C.2).

Efficiency. The selection of operating parameters results in higher stack efficiency in the stack-optimized case compared to the system-optimized case. However, concerning system efficiency, the opposite holds true. This indicates that considerations for downstream compression lead to decisions within the electrolyzer that may disadvantage its stand-alone performance but facilitate higher system efficiency within the electrolysis system.

Compared to the reference case, both optimized cases demonstrate heightened system efficiency and stack efficiency. Assuming that only the efficient stand-alone operation (and thus the stack efficiency) is pertinent for electrolyzer manufacturers and operators, adjusting pressure and temperature can yield an absolute increase in stack efficiency of approximately 4% at the nominal point, even without considering the electrolysis system. However, it is essential to consider the definition of the reference case, which assumes fixed pressure and temperature. A more in-depth discussion of the reference case follows in Section 3.3.1.

3.2. Part B: Integrated electrolysis system operational planning within energy system

Below, the results for the integrated operation of the electrolysis system within the considered energy system are presented. Initially, operational planning is examined concerning the selection of operating parameters, followed by an analysis of energy consumption and costs. Throughout the following discussions, both the reference case and the *pT*-opt case are scrutinized, considering both stack-optimized and system-optimized efficiency modes.

3.2.1. Operational planning

The temporal progression of selected operating parameters for the reference case and the *pT*-opt cases (system- and stack-optimized) are shown in Fig. 8.

Current density. In general, the operating strategies (i.e., time-variant current density) appear very similar across all cases. There are only isolated differences in current density, such as around 26 h and 90 h. In these instances, the current density and hydrogen production are highest in the reference case and lowest in the stack-optimized case. This is due to the higher gas crossover losses in the reference case, which result in less hydrogen being produced for the same current density. The stack-optimized case achieves the highest stack efficiency, resulting in the lowest gas crossover losses and the highest hydrogen production at identical current densities compared to the reference

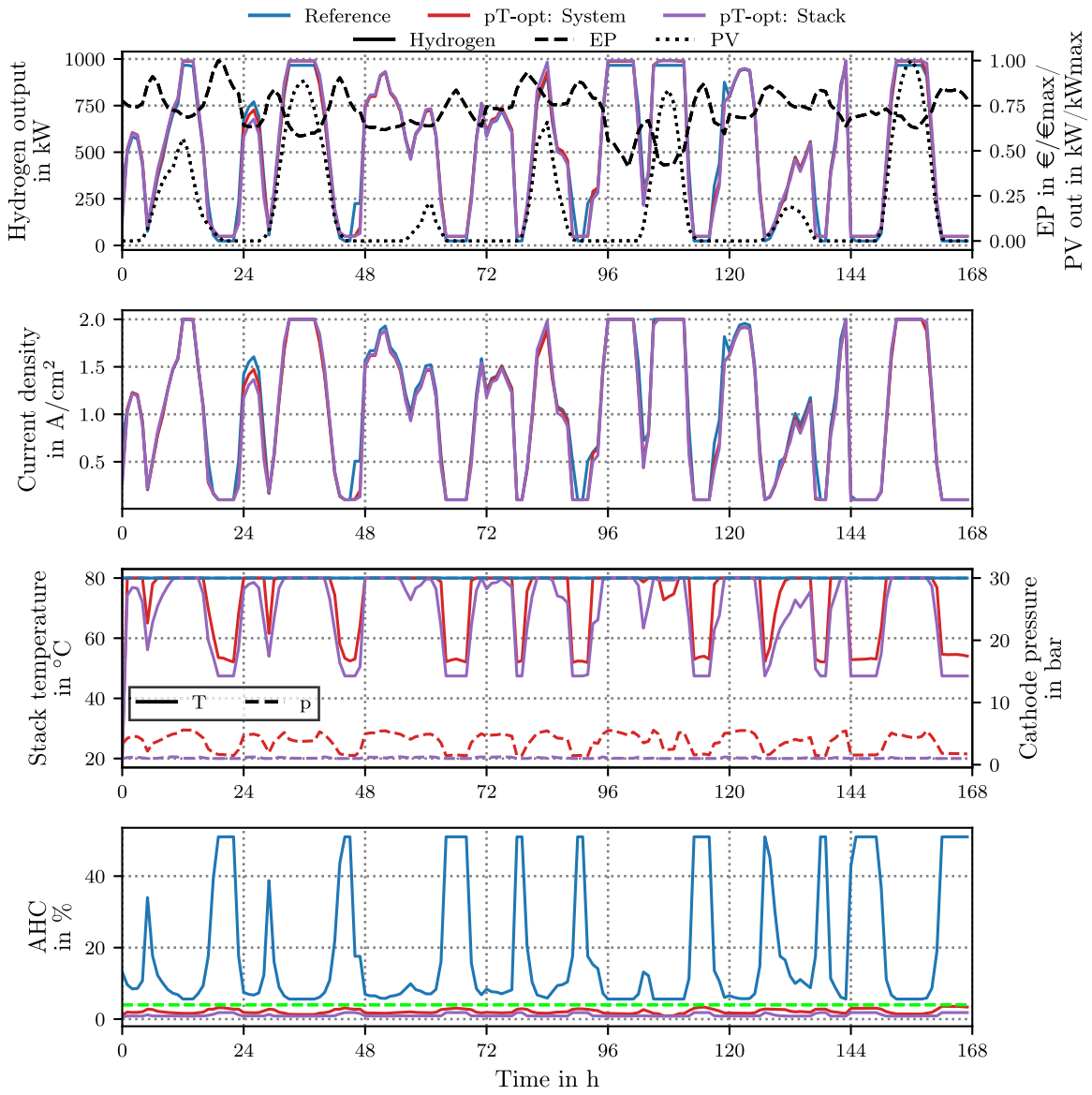

Fig. 8. Temporal progression of selected operating parameters for the reference case (blue) and the pressure- and temperature-optimized case (*pT*-opt), split into system- (red) and stack-optimized (purple) operation for an aggregated week within an energy system. The electricity price and PV output are normalized to their maximum value over the time horizon. The green dotted line indicates the safety limit of the AHC (EP: Electricity price, PV: Photovoltaic, AHC: Anodic hydrogen content).

and system-optimized cases. This pattern is also evident at times of maximum (e.g., at 100 h) and minimum current density (e.g., at 66 h). As a result, these losses must be offset by increased production at certain times.

Due to the inherently higher hydrogen yield at identical current density, it becomes feasible to select lower average current densities for both optimized cases (i.e., 1.02 A/cm^2 compared to 1.06 A/cm^2). This approach allows for the exploitation of an additional increase in efficiency, as efficiency tends to improve at lower current densities compared to higher ones (Fig. 7).

Nevertheless, the similarity of the operating strategies across all cases suggests that the optimization of operating parameters has minimal impact on operational planning regarding the time-variant hydrogen production. This production is primarily driven by the availability of PV electricity and electricity prices.

Temperature and pressure. In the system-optimized scenario, temperatures fluctuate between 52 °C and 80 °C (on average 72 °C); the maximum temperature accounts for 63% of the time period assessed here. Conversely, in the stack-optimized case, temperatures range from 45 °C to 80 °C (on average 68 °C), with the maximum temperature comprising 29% of the time.

This difference reflects the tendency to select lower temperatures for stack efficiency optimization compared to system efficiency optimization (Fig. 7). Nevertheless, for both cases, it is beneficial to enable high operating temperatures, but maintaining them continuously is not desirable in either case.

In the system-optimized case, the pressure slightly varies between 1.4 bar and 5.5 bar, with an average of 3.7 bar. In the stack-optimized case, the pressure remains close to atmospheric levels. The maximum pressure is never reached and is not relevant for either case in this study.

The largest temperature and pressure change between two adjacent time steps is approximately 30 K/h and 2.8 bar/h for both optimized cases combined. Given that PEM electrolyzers have a cold start-up time of only a few minutes [2], it is assumed that the optimized operating strategy can be realistically implemented.

Gas crossover. In contrast to the reference case, the anodic hydrogen content (AHC) remains below the limit value for the entire period in

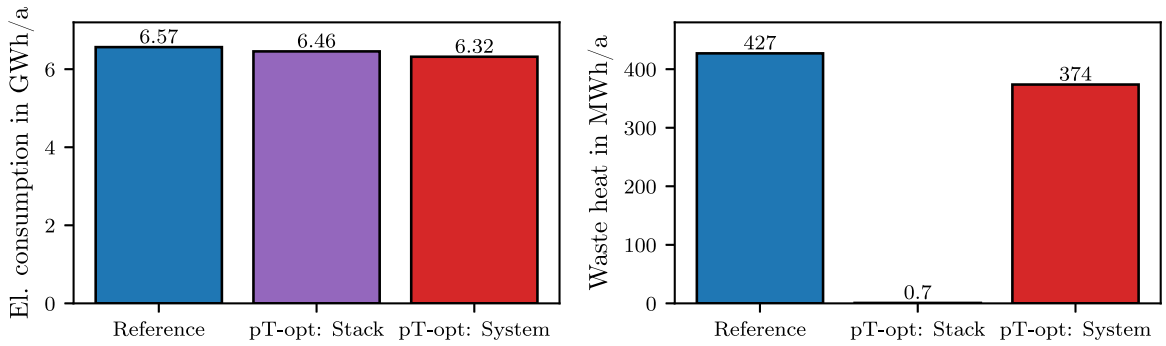

Fig. 9. Comparison of the annual electricity consumption and the annual waste heat of the PEM electrolysis system for the reference case (blue) and the pressure and temperature-optimized case (*pT*-opt), split into system- (red) and stack-optimized (purple) operation.

both optimized cases. For the reference case, it is important to note that the high peaks in AHC occur when the electrolyzer operates at minimum load. In practice, the electrolyzer would likely be switched off during these periods to avoid such high AHC levels; but this case is not captured by the process model due to its inability to simulate this discrete state.

Outside of these peak times, the limit value is also exceeded in the reference case, but to a lesser extent. In these situations, additional technical measures to reduce AHC could be implemented to stay below the limit and enable compliant operation.

3.2.2. Energy consumption

Based on the operating strategies explained above, Fig. 9 shows the resulting annual electricity consumption and the waste heat generated by the PEM electrolysis system for the reference case and the stack- and system-optimized *pT*-opt case.

Electricity consumption. The enhanced efficiency resulting from optimized operating parameters is evident in the electricity consumption of the electrolysis system. Consequently, electricity consumption can be decreased from 6.57 GWh/a to 6.46 GWh/a in stack-optimized operation and to 6.32 GWh/a in system-optimized operation compared to the reference case. This represents a reduction of 1.7 % and 3.8 %, respectively.

Waste heat. The waste heat generated follows a similar trend to the electricity consumption. In the system-optimized case, waste heat can be reduced from 427 MWh/a to 374 MWh/a compared to the reference case, corresponding to a reduction of 12.4 %.

Stack-optimized operation presents a unique case. As explained in Section 3.1.2, the electrolyzer adjusts the temperature in stack-optimized operation to balance the cell voltage and the thermobalanced voltage, thereby eliminating the need for external heating and waste heat production. This applies to operation within the considered energy system as well, resulting in only a negligible amount of waste heat of 0.7 MWh/a.

3.2.3. Costs

Fig. 10 shows the annual operating costs of the energy system under consideration for the reference case and the stack- and system-optimized *pT*-opt case.

Similar to the reductions in electricity consumption, a corresponding trend emerges here, showcasing a decrease in the energy system's operational costs. Specifically, in stack-optimized operation, costs drop from 594 k€/a to 572 k€/a, while in system-optimized operation, they decrease further to 552 k€/a, compared to the reference case. This translates to savings of 3.7 % and 7.1 %, respectively.

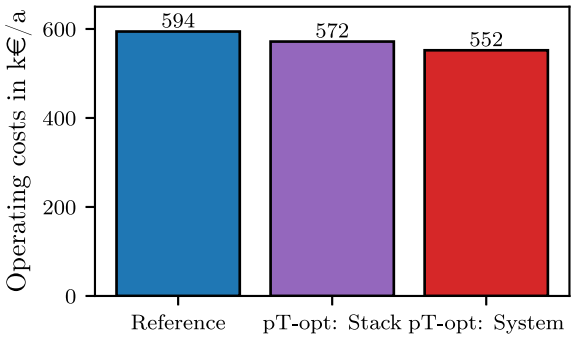

Fig. 10. Comparison of the annual operating costs for the energy system under consideration for the reference case (blue) and the pressure and temperature-optimized case (*pT*-opt), split into system- (red) and stack-optimized (purple) operation.

3.3. Discussion

The results presented above are discussed below, followed by conclusions regarding the practical implications, an assessment of the uncertainties and limitations of this work, and a potential outlook for future research.

3.3.1. Part A: Isolated electrolysis system model performance assessment

Stack-optimized operation. If no information on downstream hydrogen compression is available or if the optimization of the electrolyzers' stand-alone operation is the primary focus, optimizing the operating parameters can enhance stack efficiency by approximately 4% at the nominal point compared to the reference case. The temperature is chosen based on the thermobalanced voltage to avoid the need for external heating and associated efficiency losses. Additionally, although the hydrogen pressure, which is important from a system perspective, is minimized, the improvements in stack efficiency are sufficient to also enhance overall system efficiency. Therefore, variable adjustment of the operating parameters is beneficial from all perspectives.

System-optimized operation. Further increases in efficiency can be achi eved if the electrolyzer considers downstream compression in its operation. Compared to the reference case, the maximum system efficiency can be increased from around 70% to over 75%. At the same time, the operating range in which a satisfactory system efficiency is achieved is extended and the maximum permissible anodic hydrogen content is not exceeded. This is accomplished by raising both the pressure and temperature compared to the stack-optimized operation. While this adjustment may initially reduce stack efficiency, it improves overall system efficiency from a broader system perspective. Therefore, it is sensible to take into account the entire process chain when planning the operation of electrolyzers to realize lower production costs through

system integration, even if this means accepting electrolyzer efficiency losses.

The choice of operating parameters (pT-opt) indicates that selecting the maximum pressure is not optimal across the entire operating range, while the maximum temperature is only beneficial for medium to higher current densities. The fact that the optimal temperature differs from pure temperature optimization (T-opt) and the optimal pressure differs from pure pressure optimization (p-opt) demonstrates that the choice of these parameters is interdependent; i.e., there is always an optimal pair of temperature and pressure for effective operation.

Compared with previous studies that have investigated the selection of optimal operating parameters, the results presented here are qualitatively consistent. For the pT-opt (system-optimized) case, the trends in system efficiency, temperature, and pressure quantitatively align with the findings of Scheepers et al. [13], supporting conclusions regarding decreasing temperatures at low current densities and a slight pressure increase towards higher current densities to maximize efficiency. Tjarks et al. [18] investigated the energetically optimal pressure for PEM electrolyzer systems and reported results comparable to the p-opt case. However, their findings indicated cathode pressures approximately 5 bar higher, which may be attributed to a different membrane choice and the additional consideration of hydrogen drying.

These findings initially validate that the PEM electrolysis system model presented here is capable of replicating qualitative insights from prior studies, affirming its suitability for this study's scope. However, the optimization approach and the subdivision into the four operating modes allow for a more detailed examination of the various factors affecting the choice of optimal operating parameters. This approach ensures greater traceability compared to the cited analytical studies. Additionally, the optimization approach enables distinctions between system-optimized and stack-optimized operation without necessitating changes to the process model formulation, thereby providing a novel perspective on selecting optimal operating parameters.

Reference case. The previously mentioned improvements are in relation to a reference case. In this work, the reference case is defined with fixed cathode pressure and stack temperature across the entire operating range, reflecting a state-of-the-art electrolyzer based on current properties. This assumption is grounded in the fact that manufacturers typically specify the polarization curve, a measure of electrolyzer efficiency, at nominal pressure and temperature [2].

Furthermore, electrolyzer manufacturers often claim to produce hydrogen at a fixed pressure level, making variable pressure adjustment unlikely. The plausibility of the reference case is supported by the fact that the stack efficiency curve (Fig. 7) qualitatively and quantitatively corresponds to commonly reported curves in the literature [2,12].

However, this does not imply that electrolyzer manufacturers have not implemented progressive control of the operating parameters. Evidence for this is provided by the exceeding of the permissible anodic hydrogen content (Fig. 6), which makes operation according to the reference case impossible. For permissible operation, additional measures (e.g., adaptation of catalyst materials) are required to prevent high hydrogen accumulation at the anode.

Ultimately, the stack-optimized efficiency mode in the pT-opt operating mode represents the optimal performance a stand-alone electrolyzer (with the technical properties from Table A.1) can achieve. The current state of the art likely reflects an intermediate state between this optimal mode and the reference mode. Nonetheless, it is evident that additional efficiency gains can be achieved through a system-wide approach (system-optimized).

3.3.2. Part B: Integrated electrolysis system operational planning within energy system

The optimization of the operating parameters has no noticeable influence on the operational planning of the electrolyzer with regard to the time-variant choice of load points. The operational behavior is clearly more dependent on external factors such as the availability of renewable electricity and electricity prices. Nevertheless, the optimized operating modes tend towards lower current densities than the reference case due to a higher hydrogen yield which opens the possibility to exploit further efficiency increases of lower current densities. With regard to the choice of operating parameters, stack-optimized operation tends towards lower temperatures and pressures than in system-optimized operation. However, both together have a temporal share of the maximum temperature of 29 % to 63 %, so in both cases, it seems worthwhile to enable the highest possible temperature, but this should not be maintained permanently. A high maximum pressure is not relevant in either case.

Both optimization modes result in a reduction in energy consumption within the considered energy system. The most significant savings are achieved when hydrogen compression is factored into the operation of the electrolyzer. However, stack-optimized operation demonstrates that even without this information, energy consumption can be decreased by flexibly adjusting pressure and temperature to optimize the stand-alone electrolyzer operation. The observed reductions in energy consumption during operational planning are less pronounced than the improvements in maximum efficiency during isolated operation (Section 3.1). This discrepancy arises due to the dynamic nature of external factors, such as the availability of renewable electricity and fluctuating electricity prices, which primarily influence the selection of load points. As a result, the chosen load points vary over time, reflecting the general increase in efficiency over a wide load range rather than the increase in maximum efficiency.

Additionally, stack-optimized operation eradicates the generation of waste heat. Consequently, integrating this waste heat to further enhance system efficiency is not feasible, unlike in the system-optimized scenario where it could be considered. As the electrolysis system model is a steady state process model, the waste heat generated is balanced only in the steady state, and heating and cooling processes between adjacent time steps are not accounted for. Addressing this aspect would require a dynamic process model. However, this should have a negligible effect on the statements made so far, as the process water preheating $\dot{Q}_{heat}$ (Eq. (A.7)) has the least influence on the thermobalanced voltage (Fig. C.1).

Finally, both operational modes facilitate a reduction in annual operating costs, achieving cost savings of approximately 7% at best. Notably, in both instances, the cost savings surpass the energy savings. This discrepancy is attributed to the time-dependent nature of electricity prices, where energy savings carry varying cost weights contingent upon the time period.

The analysis of cost-optimal operating points for electrolyzers has already been addressed in the literature. For instance, Scheepers et al. [11] identified an optimal current density of 1.19 A/cm^2 under similar boundary conditions to minimize hydrogen production costs. Although this value is of a similar order of magnitude to the findings in this study, the authors assumed operation at a constant current density, thereby overlooking the potential benefits of fluctuating operation based on electricity price and availability.

While the cost savings of fluctuating operation, including temperature adjustments, were demonstrated in another study [10], that study did not account for simultaneous pressure adjustments, nor did it consider the full electrolysis system, including hydrogen compression.

Therefore, the results of this paper align with previous studies regarding integrated operation, but the scope of consideration is broadened. This approach not only enables full flexibility in selecting operating parameters but also encompasses the entire electrolysis system, facilitating a detailed distinction between stack-optimized and system-optimized operation.

3.3.3. Practical implications

Based on the findings from Sections 3.1 and 3.2, it can be concluded that adjusting the operating temperature and pressure according to the current density (i.e., depending on the load point) can improve the electrolyzer system efficiency, thereby reducing both electricity consumption and operating costs within the associated energy system. The full potential for savings can be achieved if the electrolyzer accounts for subsequent hydrogen compression during operation, adjusting temperature and pressure accordingly. For practical implementation, it is therefore crucial for an electrolyzer operator not only to optimize the electrolyzer's own efficiency but also to consider interactions with other system components. Since these components may not all be from the same manufacturer, there is likely a need for cross-technology and cross-manufacturer communication and cooperation. This could complicate real-world implementation, as new intelligent interfaces may be required between system components.

Additionally, variable adjustment of operating parameters demands complex control technology. This will likely involve both adaptations to existing control technologies and the development of new, advanced control algorithms, as discussed in [51]. This paper can serve as a foundation to enable model-based control and real-world implementation, although some further extensions are necessary for this purpose (see Section 3.3.5).

In terms of safety, the anodic hydrogen content (AHC) is a critical parameter, which should remain below 4% to prevent the formation of an explosive gas mixture [52]. This risk typically rises at low current densities as well as with increased temperatures and pressures, as high temperatures and pressures narrow the permissible load range of an electrolyzer by raising the allowable minimum current density [53]. Given the dynamic operation of electrolyzers integrated with renewable energy sources, low current densities are likely to be necessary more often to maximize renewable energy utilization. In the reference case, high AHC levels appear during these low-current periods, confirming that safe operation is restricted under such conditions.

Since dynamic optimization of the operating parameters generally favors lower temperatures and pressures, the AHC limit is consistently maintained within safe bounds. Optimizing these parameters not only enhances efficiency but also broadens the safe operational range, thereby supporting potentially greater energy and cost savings when paired with renewable energy sources.

With respect to degradation, high temperatures, pressures, and current densities accelerate wear. Since the optimization of operating parameters tends to favor lower values for current density, pressure, and temperature, this dynamic adaptation not only improves efficiency but also generally reduces degradation based on the respective average levels [54,55].

However, the findings also indicate that temporal variation in operating parameters creates larger temperature and pressure gradients, which may introduce higher mechanical and thermal stresses, potentially increasing degradation. The effects of dynamic operation on degradation remain uncertain overall [56], and further investigation is needed, particularly regarding the impact of temperature and pressure fluctuations.

3.3.4. Uncertainties

The PEM electrolysis system model developed here is based on both thermophysical and technical properties. The parameters used are derived from both physically defined material properties and technical specifications, primarily characterizing the polymer electrolyte membrane. These values are generally determined experimentally, introducing uncertainties associated with the test specimen and experimental setup. As a result, reference values, such as those for the exchange current density $j_{0,ref}$, vary in the literature [37]. This study consciously limits the selection of parameter references to ensure consistency and facilitate model validation (Table A.1).

The choice of membrane, and consequently the membrane thickness, exerts the greatest influence on the results. For this reason, a sensitivity analysis is conducted in Appendix D.1 for a commercially available membrane thickness of 180 µm (Nafion N117) as opposed to 51 µm (Nafion N212) in the main text. While efficiency curves and optimal operating parameters show slight quantitative changes, the qualitative trends (i.e., increased efficiency with adjustments to pressure and temperature, non-optimal maximum temperatures at low current densities, and a slight pressure increase with rising current density) remain valid for different membrane thicknesses. This underlines the robustness of the key findings of this article.

Concerning integrated operation within an energy system, the main uncertainties arise from the energy system configuration and the energy prices considered. To ensure validity regarding system structure, a configuration (i.e., component selection and sizing) was chosen based on prior studies that identified this setup as cost-optimal for hydrogen production from electrolyzers [47]. This reflects an energy system configuration likely to be implemented in future applications.

To evaluate the impact of energy prices (i.e., electricity prices) on integrated operation, a sensitivity analysis is performed for the years 2019 (low electricity prices) and 2022 (high electricity prices) in Appendix D.2. Although the absolute operating costs vary, the relative energy and cost savings compared to the reference case are consistent with the main analysis. This finding demonstrates that the primary conclusions of this study are robust regarding both cost and energy savings.

3.3.5. Limitations and outlook

Each component within an electrolyzer exhibits inertia, meaning that sudden load changes lead to deviations from steady-state conditions (e.g., variations in temperature and pressure from target values) [57]. Since the electrolysis system model presented in this paper operates under steady-state assumptions, it cannot capture these transient deviations. However, these steady-state conditions are typically reached within a few minutes [57]. Given the hourly resolution used in this analysis, such deviations should have minimal impact on the overall results.

In a real-world implementation linked with renewable energy sources, load changes may occur over shorter intervals, requiring that these deviations be adequately managed by a responsive control strategy. In particular, dynamic adjustment of the target temperature could be beneficial here; leveraging natural temperature drops from load changes could enable efficient operation at lower loads without requiring the heat management system to counteract these drops [57]. While the dynamic operation of an electrolyzer alongside renewable energy does necessitate a complex, tailored control system, this need exists independently of the dynamic operating parameter adjustments presented in this paper. Instead, these adjustments can be integrated into control strategies as supportive measures, acting more as an asset than an additional constraint.

The proposed electrolysis system model can serve as a foundation for designing a controller that leverages the benefits of dynamically adjusting operating parameters. However, the electrolysis system model must account for component inertia and other time-dependent uncertainties, necessitating a dynamic model, such as that described in [58], rather than a steady-state approach. The scope of this paper is limited to demonstrating the potential of dynamic operating parameter adjustments, for which a steady-state model suffices. Further development toward a dynamic model could be explored in future work.

Furthermore, this paper examines the optimization of operational parameters and the associated reduction in operating costs. However, investment costs are also critical for cost-effective hydrogen production, with electrolyzer system sizing playing a significant role in determining these investment costs. The effect of operational parameter optimization on investment costs is not addressed in this study. However, two considerations are important here. First, the baseline configuration of

the energy system under consideration is a cost-optimal design that incorporates investment costs. Second, it is shown that operational parameter optimization has minimal impact on the operating strategy (i.e., the timing and intensity of current density application, thereby dictating when and how much hydrogen is produced). This suggests that the capacity of the electrolyzer system does not need to be adjusted as a result of optimizing operational parameters.

As electrolyzer investment costs are projected to decline in the coming years, the proportion of electricity costs within hydrogen production expenses could rise to as much as 90% [9]. Thus, even the relatively modest electricity savings of 4% demonstrated in this paper through the proposed optimization strategies could significantly contribute to further reducing hydrogen production costs, particularly in the future.

Although this study considers a cost-optimal energy system configuration, applying the PEM electrolysis system model presented here to other case studies could prove beneficial. Such applications would allow the exploration of operating parameter optimization for varying electricity supplies or hydrogen demands, as well as the potential for waste heat utilization to enhance overall energy system efficiency. For economic evaluation, the presented model can be applied in further case studies with larger capacities to investigate scalability and to facilitate a comparison of investment costs and operating cost reductions on an industrial scale. In this context, it is important to note that although the process model was developed for a nominal capacity of 1 MW, all effects were analyzed based on current density, which is independent of the electrolyzer's capacity. Therefore, the findings can be equivalently transferred to both larger and smaller scales.

4. Summary and conclusion

Hydrogen has the potential to play a pivotal role in the ongoing transformation of the energy supply, yet its production via electrolyzers remains prohibitively expensive. One strategy to reduce operating costs of electrolyzers is to enhance operating efficiency by optimizing the interaction of the operating parameters (i.e., current density, temperature, and pressure).

To this end, this paper presents a novel equation-oriented process model of a PEM electrolysis system including the electrolyzer and downstream hydrogen compression. Using this model, the performance of the electrolysis system is initially analyzed in isolation by optimizing its operating parameters through operational flowsheet optimization. The process model is subsequently integrated into an overarching energy system, where its operating parameters are optimized as part of an operational planning optimization. The main findings can be summarized as follows.

- Optimizing the operating parameters, compared to an operating mode with fixed temperature and pressure at their maximum values, increases the maximum system efficiency by about 5 %pt. while shifting this maximum more significantly towards lower current densities. Consequently, this broadens the usable operating range with sufficiently high system efficiency.
- For each current density, there exists an optimal pair of operating pressure and temperature in terms of efficiency. The maximum operating temperature proves to be optimal only at loads exceeding 40%; however, the maximum operating pressure does not exhibit optimal behavior regarding system efficiency.
- The optimal temperature and pressure vary depending on whether optimizing for overall system efficiency or electrolyzer stack efficiency. For achieving optimal system efficiency, it is observed that greater losses within the electrolyzer are tolerated in exchange for improved overall system efficiency through a more efficient hydrogen compression.
- When knowing information about the hydrogen post-compression, optimizing the operational parameters within the electrolyzer with regard to system efficiency can lead to reductions in energy consumption (4%) and operating costs (7%) for the considered energy system. Even without compression information, optimizing operational parameters with regard to electrolyzer stack efficiency can reduce energy consumption (2%) and operating costs (4%).
- Optimizing the operating parameters toward lower values tends to yield additional positive side effects. This approach ensures a safe anodic hydrogen content across the entire operating range, potentially extending the permissible operating range.
- The operating strategy, expressed by the time-variable choice of current density, does not differ noticeably between the examined cases. However, the choice of the operating parameters temperature and pressure influences gas crossover losses, yielding different hydrogen production rates at the same current density. Consequently, optimal operating strategies differ in certain time steps. Therefore, models that can reflect these relationships are needed to find the optimal operating strategy of electrolyzer systems.

In summary, the results of this study indicate that continuous operation of a PEM electrolyzer at maximum temperature and pressure is not necessarily the most efficient approach. Instead, efficiency can be improved by optimally adjusting temperature and pressure according to the current density. Fully realizing this potential requires consistently evaluating the electrolyzer within the broader energy system context. Implementing strategies that may initially introduce higher inefficiencies at the electrolyzer level can ultimately deliver greater benefits within the overall electrolysis system, leading to significant energy and cost savings at the energy system level.

These findings offer promising advancements for green hydrogen technologies, supporting more cost-effective green hydrogen production. However, they also highlight the need for advanced operating strategies that facilitate cross-technology and cross-manufacturer collaboration throughout the hydrogen value chain. Such an approach is essential for achieving meaningful reductions in green hydrogen production costs.

Despite these positive outcomes, certain limitations of the study are acknowledged. The proposed operating strategy introduces complexity, as it requires sophisticated control systems to manage dynamic operating conditions. This necessitates dynamic models capable of accommodating system uncertainties and inertia, which become particularly relevant when combined with the fluctuating supply of renewable energy. While the presented PEM electrolysis model does not account for these factors, it serves as a foundation for developing a dynamic model that could address these aspects in future studies. Therefore, advancements in automation and control technologies will be critical for applying these findings in practical scenarios.

Further case studies could yield additional insights, for instance, by integrating waste heat utilization within the energy system alongside optimization of operating parameters to achieve additional systemic energy savings and assess its impact on parameter selection.

Moreover, this study focuses solely on operating cost reduction. For a comprehensive economic evaluation of hydrogen production costs, it is essential to consider investment costs and system design. The insights gained from optimizing operating parameters could thus be incorporated into a full economic assessment in subsequent studies.

In conclusion, this paper demonstrates a promising approach to reducing the operating costs of hydrogen-based energy systems through optimized operating strategies alone, without requiring additional technical advancements in PEM electrolyzer design.

CRediT authorship contribution statement

Luka Bornemann: Writing – original draft, Visualization, Software, Methodology, Formal analysis, Data curation, Conceptualization. **Jelto Lange:** Writing – review & editing, Supervision, Conceptualization. **Martin Kaltschmitt:** Writing – review & editing, Supervision, Funding acquisition, Conceptualization.

Declaration of Generative AI and AI-assisted technologies in the writing process

During the preparation of this work the authors used ChatGPT in order to improve readability and language. After using this tool/service, the authors reviewed and edited the content as needed and take full responsibility for the content of the publication.

Declaration of competing interest

The authors declare that they have no known competing financial interests or personal relationships that could have appeared to influence the work reported in this paper.

Acknowledgments

This research is supported by the German Federal Ministry for Economic Affairs and Climate Action under the 'Green hydrogen for Lübeck's mobility of tomorrow - Hydrogen supply for the operation of a waste collection vehicle under a holistic use of all side streams - Subproject Modeling and Assessment' (HyHL) project with the funding code 03EI3055D. The support is gratefully acknowledged. Furthermore, the authors express their gratitude to Arne Kaufmann and thank him for his helpful cooperation in the preparation of this paper.

Appendix A. Mathematical formulation

The mathematical formulation of the electrochemical model for the electrolysis system is detailed in Appendix A.1 below. Additionally, the modeling of the energy system is described in Appendix A.2.

A.1. Electrochemical model

A.1.1. Voltage

The cell voltage U_{cell} must be applied to the electrolysis cell for the electrolysis reaction to occur. This voltage consists of the open-circuit voltage U_{ocv}, the activation overvoltage U_{act}, and the ohmic overvoltage U_{res} (Eq. (4) [38]). Diffusion overvoltages are neglected.

$$U_{cell} = U_{ocv} + U_{act} + U_{res} \tag{A.1}$$

The open-circuit voltage U_{ocv} is calculated via the Gibbs energy using the IDAES platform (Eq. (A.2) [38]).

$$U_{ocv} = \frac{\Delta G}{zF} = \frac{G_{H_2,c} + 0.5G_{O_2,a} - G_{H_2O,l}}{zF} \tag{A.2}$$

With the Faraday constant F, the number of electrons z, and the Gibbs energy of the hydrogen at the cathode $G_{H2,c}$, the oxygen at the anode $G_{O2,a}$ and the added liquid water $G_{H2O,l}$.

The activation overvoltage is calculated by using a approximation of the Tafel equation Eq. (A.3) with the gas constant R, stack temperature T_{stack}, charge transfer coefficient α, current density j and current exchange density j_0. It is assumed that the cathodic activation overvoltage is smaller than the anodic overvoltage and therefore neglected (i.e., the activation overvoltage only considers the anodic activation overvoltage) [13].

$$U_{act} = \frac{RT_{stack}}{\alpha zF} \ln\left(\frac{j}{j_0}\right) \tag{A.3}$$

Furthermore, the temperature dependence of the anodic current exchange density j_0 can be expressed as a function of the activation energy E_A, the stack temperature T_{stack}, and the reference exchange density $j_{0,ref}$ at the reference temperature T_{ref} (Eq. (A.4) [13]).

$$j_0 = j_{0,ref} \exp\left(-\frac{E_A}{RT_{stack}}\left(1 - \frac{T_{stack}}{T_{ref}}\right)\right) \tag{A.4}$$

The ohmic overvoltage U_{res} can be expressed using Ohm's law and depends on the interface resistance R_0, the membrane thickness d_m, the membrane swelling factor δ_m and the membrane resistance σ_m (Eq. (A.5) [13]).

$$U_{res} = \left(R_0 + \frac{d_m\delta_m}{\sigma_m}\right) j \tag{A.5}$$

The temperature dependence of the membrane resistance σ_m can be expressed as a function of the water activity within the membrane a_{H_2O} (Eq. (A.6) [13]).

$$\sigma_m = \left(0.6887 + a_{H_2O}\right)^3 \exp\left(\frac{-10440 a_{H_20}^{0.25}}{RT_{stack}}\right) \tag{A.6}$$

The validation of the cell voltage is shown in Fig. B.3.

A.1.2. Heat management

During the electrolysis reaction, two opposing processes occur in the cell that influence heat management.

- Heat is generated by the ohmic overvoltages and activation overvoltages, which heat up the cell.
- The phase change from liquid water to gaseous hydrogen and oxygen, as well as the vaporization of water, requires enthalpy of vaporization, which cools the cell.

In addition, heat must be used to preheat the process water to the desired stack temperature [12]. These relationships are expressed via the thermobalanced voltage U_{tb} (Eq. (A.7) [12]). This depends on factors such as the thermoneutral voltage U_{tn}, water preheating $\dot{Q}_{heat}$, and the evaporation energy of the water vapor H_{ev}^{gas}.

$$U_{tb} = U_{tn} + \frac{\dot{Q}_{heat}}{2F} + \frac{H_{ev}^{gas}}{2F} \tag{A.7}$$

The thermoneutral voltage corresponds to the ideal voltage for the electrolysis reaction to take place when all the necessary reaction energy is provided entirely by electrical energy [37]. It is calculated using the enthalpies of the species involved (Eq. (A.8)).

$$U_{tn} = \frac{\Delta H}{zF} = \frac{H_{\mathrm{H_2},c} + 0.5H_{\mathrm{O_2},a} - H_{\mathrm{H_2O},l}}{zF} \tag{A.8}$$

The heat required to preheat the process water $\dot{Q}_{heat}$ is calculated as the product of the amount of water that reacts $\dot{n}_{\mathrm{H_2O}}^{reac}$ and evaporates $\dot{n}_{\mathrm{H_2O}}^{vap}$ (i.e., the amount of water which leaves the system boundary) and the enthalpy difference between the inlet and outlet of the preheater $\Delta H_{preheat}$, relative to the amount of hydrogen produced $\dot{n}_{\mathrm{H_2}}^{tot}$ (Eq. (A.9)).

$$\dot{Q}_{heat} = \frac{\dot{n}_{\mathrm{H_2O}}^{reac} + \dot{n}_{\mathrm{H_2O}}^{vap}}{\dot{n}_{\mathrm{H_2}}^{tot}} \Delta H_{preheat} \tag{A.9}$$

The energy content of the water vapor H_{ev}^{gas} is calculated as the product of the amount of water vapor at the anode $\dot{n}_{\mathrm{H_2O},a}$ or cathode $\dot{n}_{\mathrm{H_2O},c}$ and the enthalpy of vaporization $H_{vap,i}$, relative to the amount of hydrogen produced (Eq. (A.10)).

$$H_{ev}^{gas} = \frac{\dot{n}_{\mathrm{H_2O},a}\Delta H_{vap,a} + \dot{n}_{\mathrm{H_2O},c}\Delta H_{vap,c}}{\dot{n}_{\mathrm{H_2}}^{tot}} \tag{A.10}$$

A.1.3. Gas crossover

According to Fick's law, the diffusion of oxygen or hydrogen $\dot{n}_i^{diff}$ can be expressed as a function of the temperature-dependent permeability of the membrane ϵ_i, the fugacity difference between the anode and cathode Δf_i, the membrane thickness $d_m\delta_m$, and the active cell area A (Eq. (A.11) [28]).

$$\dot{n}_i^{diff} = \epsilon_i(T)\, A \frac{\Delta f_i}{d_m\delta_m}, \quad \forall i \in \{\mathrm{H_2}, \mathrm{O_2}\} \tag{A.11}$$

Table A.1
Overview of the parameters used in the electrochemical submodel.

Parameter	Value	Unit	Ref.
z	2		
F	96 585	C/mol	
A	398 750	cm^2	
α	0.51		own fit
R	8.3144	J/(mol K)	
E_A	40 000	J/mol	[13]
$j_{0,ref}$	8×10^{-6}	A/cm^2	[13]
T_{ref}	353.15	K	[13]
R_0	27×10^{-3}	$\Omega\,cm^2$	[13]
d_m	51	µm	[13]
δ_m	1.15		[13]
a_{H_2O}	1		[13]
Y	2	bar cm^2/A	[12]
p_{use}	200	bar	[18,35]
n_{stages}	5		
η_{mech}	0.9		[18]

The material-specific permeabilities were adjusted based on the temperature dependence in Schalenbach et al. [32] (Eq. (A.12)). The validation of the gas crossover can be found in Figs. B.1 and B.2.

$$\begin{aligned}\epsilon_{H_2} &= 1.9 \times 10^{-17}\ \text{mol}/(\text{cm s Pa}) \exp(0.0225/\text{K}T_{stack}) \\ \epsilon_{O_2} &= 3 \times 10^{-19}\ \text{mol}/(\text{cm s Pa}) \exp(0.0191/\text{K}T_{stack})\end{aligned} \tag{A.12}$$

A.1.4. Compression

In the process model, compression is modeled as a single-stage isentropic compression including pre- and post-cooling. The total compression power P_{comp} is thus the result of the single-stage compression power P^1_{comp} multiplied by the number of compression stages n_{stages} (Eq. (A.13)).

$$P_{comp} = n_{stages} P^1_{comp} \tag{A.13}$$

The compression power of single-stage compression is calculated according to the IDAES Platform [30] for isentropic conditions using the enthalpy balances and the mechanical efficiency (Eq. (A.14)).

$$P^1_{comp} = \frac{\sum_i H_{isentropic} - \sum_i H_{in}}{\eta_{mech}}, \qquad \forall i \in \{H_2, H_2O\} \tag{A.14}$$

A.1.5. Material and technical properties

The parameters used explicitly for the electrochemical submodel can be found in Table A.1. In addition, ideal gas behavior was assumed as the equation of state for the calculation of gas phase properties. The molar enthalpy, molar entropy, and molar heat capacity for all gaseous substances are derived from the relationships provided by Linstrom [59]. The molar enthalpy, molar entropy, molar heat capacity, and molar density for liquid water are obtained from Poling et al. [60]. The calculation of the saturated vapor pressure of water and oxygen is based on Linstrom [59] and Perry and Green [61], respectively. Furthermore, vapor–liquid equilibrium relationships from Burgard et al. [62] are utilized.

A.2. Energy system model

The electrical power generated by the PV system $\dot{E}_{PV,t}$ at each time step t is calculated as the product of the relative power $\dot{E}_{out,rel,t}$ (see Fig. 4) and the installed nominal capacity E^N_{PV}.

$$\dot{E}_{PV,t} = \dot{E}^{rel,out}_t E^N_{PV} \tag{A.15}$$

The output power of the hydrogen storage is constrained by both relative lower and upper limits $\dot{E}^{rel,min/max}_{H2S}$ (Eq. (A.16)).

$$\dot{E}^{rel,min}_{H2S} E^N_{H2S} \le \dot{E}^{out}_{H2S,t} \le \dot{E}^{rel,max}_{H2S} E^N_{H2S} \tag{A.16}$$

Besides the input and output power, the hydrogen storage has additional variables $SOC_{H2S,t}$ that represent the state of charge. To calculate the state of charge, time-coupling constraints are introduced, linking the state of charge between two adjacent time steps. The state of charge of the subsequent time step $SOC_{H2S,t+1}$ is calculated according to Eq. (A.17). It is based on the current state of charge $SOC_{H2S,t}$, and the charge $\dot{Q}^{in}_{H2S,t}$ and discharge rate $\dot{Q}^{out}_{H2S,t}$ including the associated efficiencies η^{charge}_{H2S} and $\eta^{discharge}_{H2S}$.

$$SOC_{H2S,t+1} = SOC_{H2S,t} + \Delta t \left(\dot{E}^{in}_{H2S,t} \eta^{charge}_{H2S} - \dot{E}^{out}_{H2S,t} \frac{1}{\eta^{discharge}_{H2S}} \right) \qquad \forall t \in \mathcal{T} \tag{A.17}$$

Furthermore, the state of charge $SOC_{H2S,t}$ is limited by relative lower SOC^{min}_{H2S} and upper bound SOC^{max}_{H2S} in Eq. (A.18).

$$SOC^{min}_{H2S} E^N_{H2S} \le SOC_{H2S,t} \le SOC^{max}_{H2S} E^N_{H2S} \qquad \forall t \in \mathcal{T} \tag{A.18}$$

Table A.2
Hydrogen storage parameters.

Parameter	Value	Ref.
$\dot{E}^{rel,min}_{H2S}$	0	
$\dot{E}^{rel,max}_{H2S}$	0.3	
SOC^{min}_{H2S}	0.11	Equivalent to 20 bar [63]
SOC^{max}_{H2S}	1	
$\eta^{(dis)charge}_{H2S}$	1	

The associated parameters can be found in Table A.2. Additionally, the formulation by Kotzur et al. [48] is employed to facilitate storage across days despite the aggregated and non-chronological time series. Further information can be found in the corresponding paper.

Appendix B. Validation

The validation of the electrochemical model with regard to the gas crossover and the cell voltage is presented below.

B.1. Gas crossover

See Figs. B.1 and B.2.

B.2. Cell voltage

See Fig. B.3.

Appendix C. Further results

Further results that go beyond the main text are listed below.

C.1. Part A: Isolated electrolysis system model performance assessment

See Figs. C.1 and C.2.

Appendix D. Sensitivity analysis

To investigate the influence of key parameters regarding the results, a sensitivity analysis is conducted for both parts below.

D.1. Part A: Isolated electrolysis system model performance assessment

The PEM electrolysis system model is based on the parameters listed in Table A.1. These parameters represent material properties characteristic of polymer electrolyte membranes and are therefore not subject to modification. The variable parameter, which distinguishes PEM electrolyzers, is the membrane thickness. In the main section, a membrane thickness d_m of 51 µm was used, as indicated in Table A.1. For this sensitivity analysis, a membrane thickness d_m of 180 µm is considered, representing a commonly used Nafion N117 membrane.

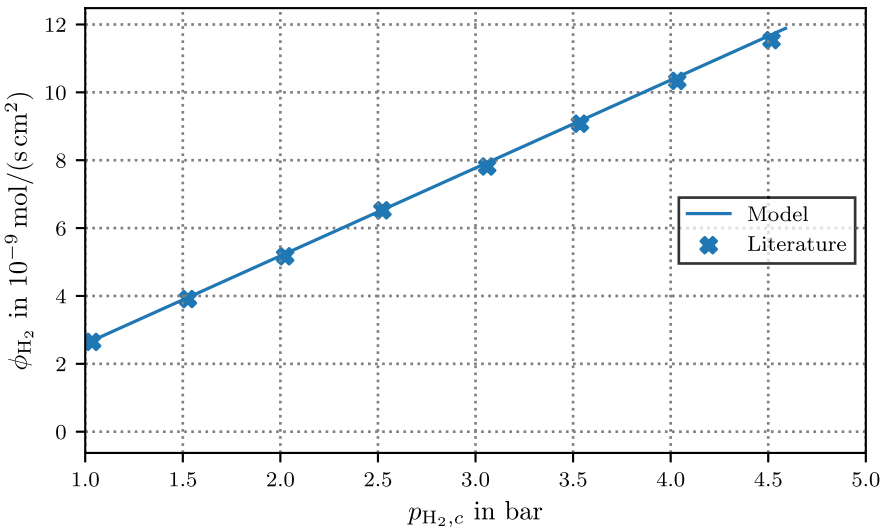

Fig. B.1. Validation of hydrogen flux density ϕ_{H_2} through the PEM calculated by the PEM electrolysis system process model against literature data provided by Schalenbach et al. [32]. This validation is carried out for a Nafion N117 membrane ($d_m = 180\,\mu m$) at a stack temperature of 80 °C by varying the hydrogen partial pressure at the cathode $p_{H_2,c}$. Since this investigation is independent of the current density, the proportionality factor Y is set to 0.

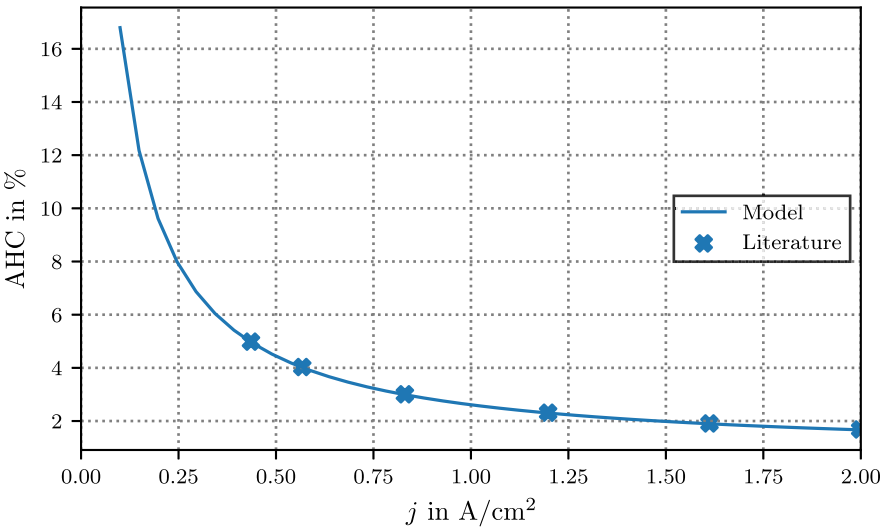

Fig. B.2. The anodic hydrogen content (AHC) is validated against literature data provided by Schalenbach et al. [12]. This validation is conducted using a Nafion N212 membrane ($d_m = 51\,\mu m$) at a stack temperature of 80 °C, with a cathode pressure of 6 bar, while varying the current density j.

Fig. D.1 shows the system efficiency, operating parameters, and other key metrics for the four operating modes with a membrane thickness of 180 µm. Section 3.1 already explained this figure in detail for a membrane thickness of 180 µm, so here only the main similarities and differences for the '*pT*-opt' case are discussed.

In terms of efficiency, the 180 µm membrane exhibits similar qualitative trends, with the '*pT*-opt' case improving system efficiency across the entire load range compared to the reference case. However, in the reference case, system efficiency reaches its maximum at a significantly lower current density, making the shift of the maximum efficiency towards lower current densities less pronounced in the '*pT*-opt' case. Despite this, the maximum efficiency is still improved by approximately 4 %pt.. A sharp decline in system efficiency at higher current densities is also observed, which is less pronounced with the 51 µm membrane. This characteristic makes the 51 µm membrane more suitable for electrolysis systems with high rated power, hence its selection for the main part of this paper.

Regarding temperature, it can be seen that a drop in temperature at lower current densities occurs and therefore maintaining the maximum temperature over a broader load range is optimal. Nevertheless, the same qualitative trends are observed. The same applies to pressure selection. Although the pressure profile's shape is similar for both membrane thicknesses, the pressure increases to just over 10 bar for the 180 µm membrane at high current densities, compared to around 6 bar for the 51 µm membrane. Even so, it is evident that reaching maximum pressure is not optimal.

Fig. D.2 shows the system and stack efficiency, as well as the temperature and pressure curves for the reference case and the two '*pT*-opt' cases for the 180 µm membrane. Similar to the 51 µm membrane, both optimized operating modes increase stack efficiency compared to the reference case, with stack-optimized operation yielding the highest stack efficiency. In terms of system efficiency, the system-optimized mode shows improved efficiency across the entire load range compared to the reference case. However, in the stack-optimized operation, a notable characteristic is observed: although stack efficiency increases throughout, system efficiency for medium to high loads falls below that of the reference case. Therefore, for a membrane thickness of 180 µm,

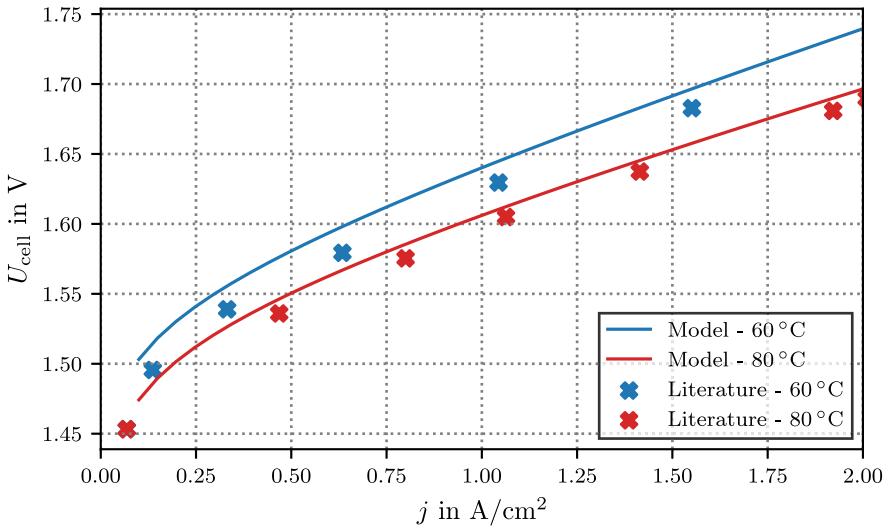

Fig. B.3. The cell voltage U_{cell} is validated against literature data provided by Scheepers et al. [13]. This validation is conducted using a Nafion N212 membrane ($d_m = 51\,\mu m$) at a stack temperature of 60 °C and 80 °C, with a cathode pressure of 2 bar, while varying the current density j.

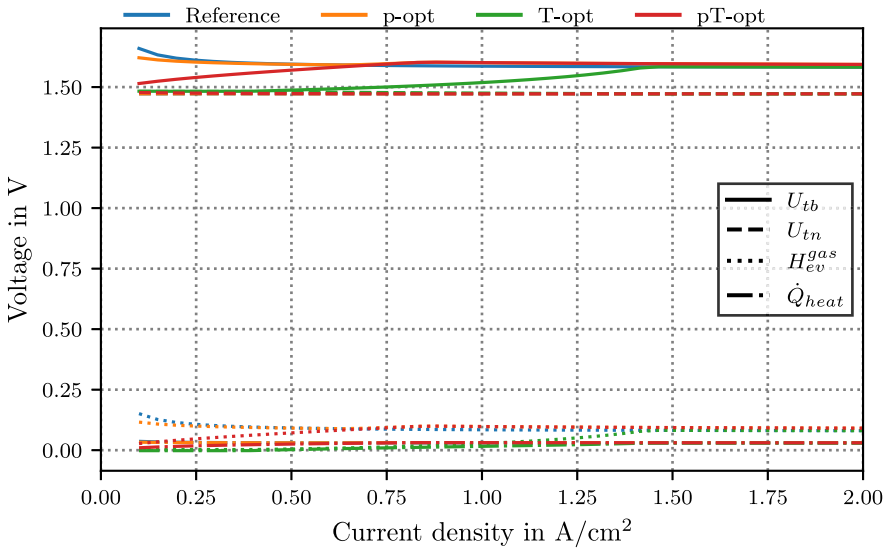

Fig. C.1. Thermobalanced voltage U_{tb} and it's parts thermoneutral voltage U_{tn}, water preheating $\dot{Q}_{heat}$, and the evaporation energy of the water vapor H_{ev}^{gas} for the various operating modes. The aim of the optimization is to maximize system efficiency η_{sys}, including compression to 200 bar (system-optimized). All values are converted into voltages according to Eq. (A.7).

it is crucial from a system perspective to include compression in the operational planning to avoid less efficient operation than the reference case.

Regarding the operating parameters, the same qualitative trends emerge as with the 51 µm membrane. Pressure is near atmospheric conditions, and temperature drops towards lower loads. However, the temperature drops only at low loads, and thus, similar to system-optimized operation, the maximum temperature represents the optimal choice for a much larger load range.

Concluding, it can initially be noted that the 180 µm membrane exhibits a different efficiency curve compared to the 51 µm membrane (i.e., a maximum at lower current densities and a steeper decline at higher current densities). Despite these differences, the same qualitative effects and benefits of temperature- and pressure-optimized operation are evident. System efficiency can be increased across the entire load range, with peak efficiency also improving by 4 %pt.. To achieve this, the temperature is reduced at low current densities, while the pressure gradually increases at higher current densities. However, it becomes apparent that the maximum temperature is optimal over a broader operating range, with pressure at the nominal point increasing by approximately 4 bar, compared to the .

Particularly for system-optimized operation, all major conclusions from the main section can also be applied to a membrane thickness of 180 µm, reinforcing the robustness of these findings. For stack-optimized operation, however, it is important to note that while beneficial under certain conditions, it may lead to less efficient operation of the PEM electrolysis system at medium to high loads from a system-level perspective.

D.2. Part B: Integrated electrolysis system operational planning within energy system

The composition and design of the energy system under consideration is intentional. On the one hand, the basic structure reflects an decentral energy system that is highly likely to be implemented

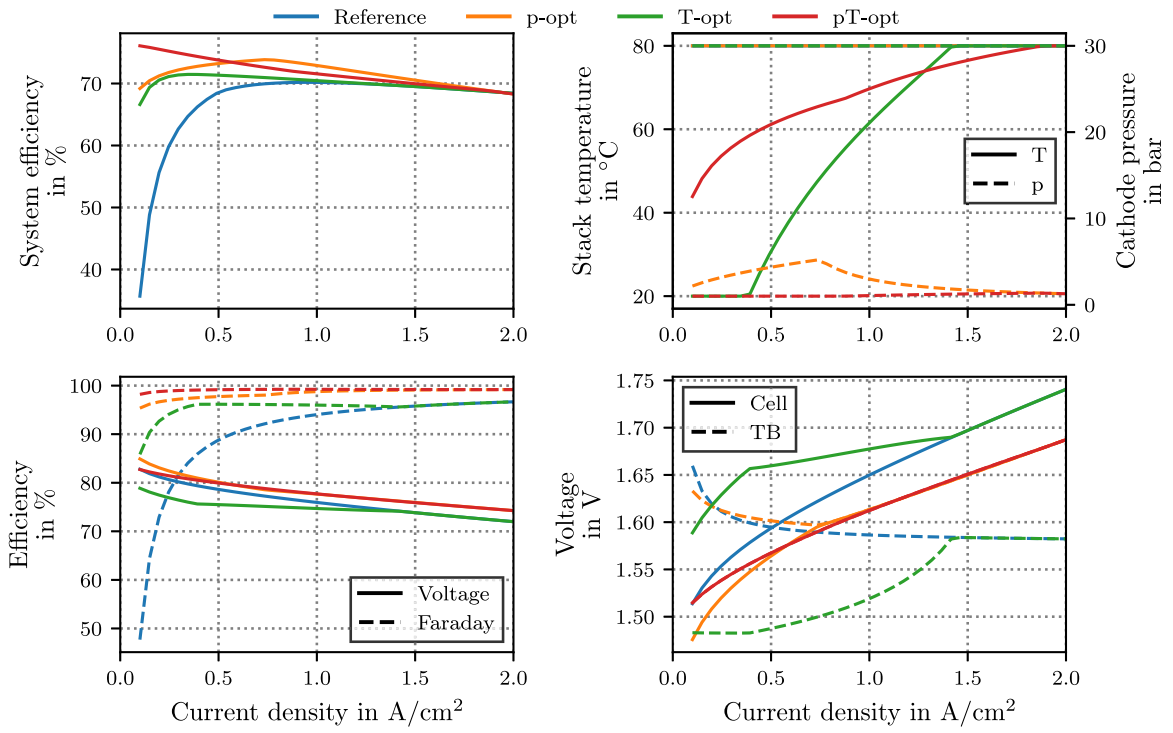

Fig. C.2. Optimal operating parameters and efficiencies for the various operating modes. The aim of the optimization is to maximize stack efficiency η_{stack} (stack-optimized) (TB: Thermobalanced).

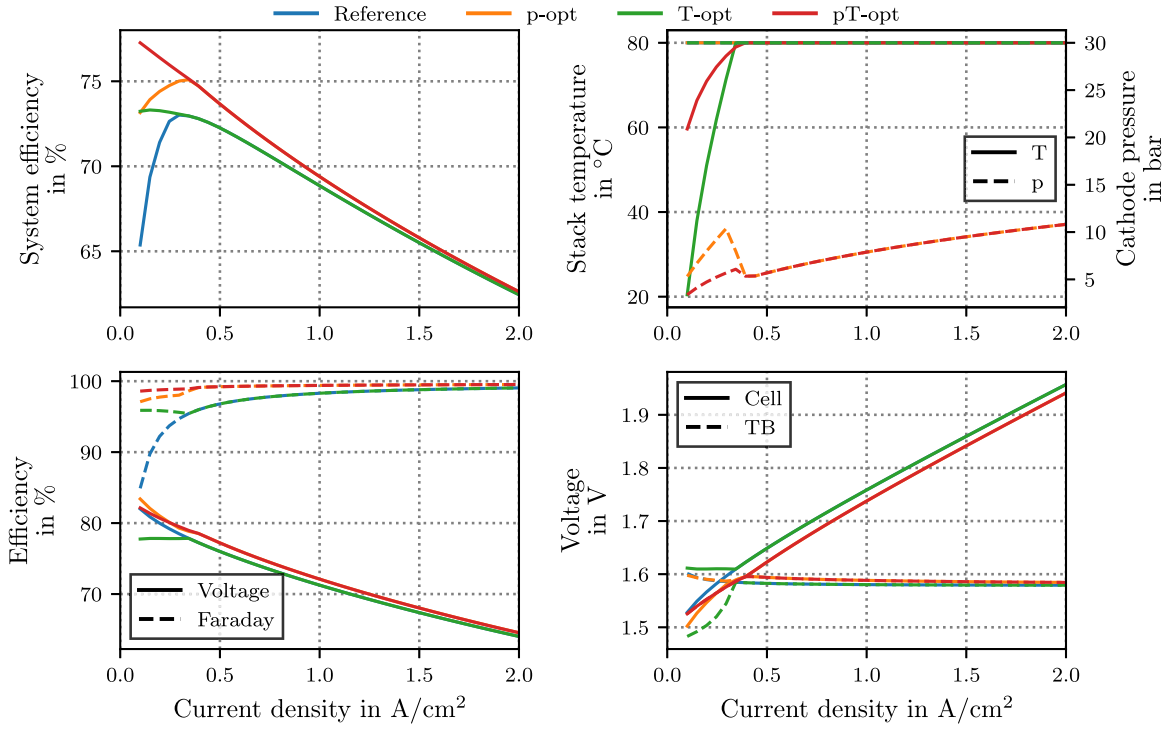

Fig. D.1. Optimal operating parameters and efficiencies (depicted by hatching) for the various operating modes (depicted by color). The aim of the optimization is to maximize system efficiency η_{sys}, including compression to 200 bar (system-optimized). The results are displayed for a membrane thickness d_m of 180 µm (Nafion N117) (TB: Thermobalanced).

in practice for hydrogen production using electrolyzers. On the other hand, the system design (i.e., the ratios of installed PV, electrolyzer capacity, hydrogen storage, and hydrogen demand, representing electrolyzer full-load hours) was based on literature results [47] to ensure a cost-optimized configuration and realistic representation. For these reasons, these parameters were not altered in the sensitivity analysis. Instead, the sensitivity analysis focuses on the underlying electricity price, which is critical for cost-effective hydrogen production. In addition to the most recent data presented in the main text, electricity prices for the years 2022 and 2019 were included in the sensitivity analysis

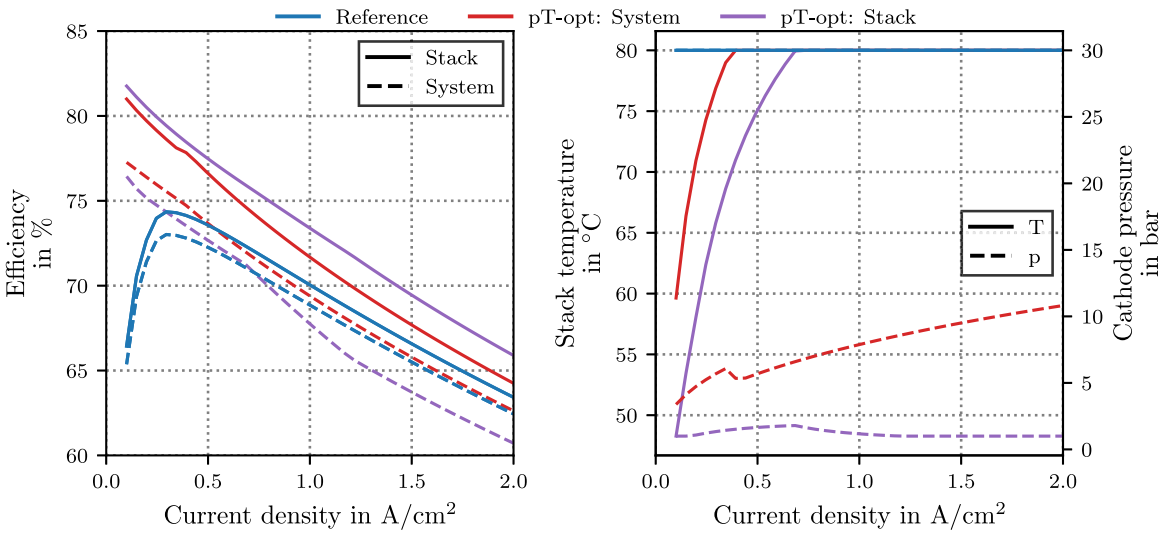

Fig. D.2. Comparison of stack and system efficiency and choice of operating parameters (depicted by hatching) for different current densities when either stack efficiency (purple) or system efficiency (red) including downstream compression is optimized. Only the simultaneous pressure and temperature optimized case (pT-opt) and the reference case are illustrated. The results are displayed for a membrane thickness d_m of 51 µm (Nafion N117).

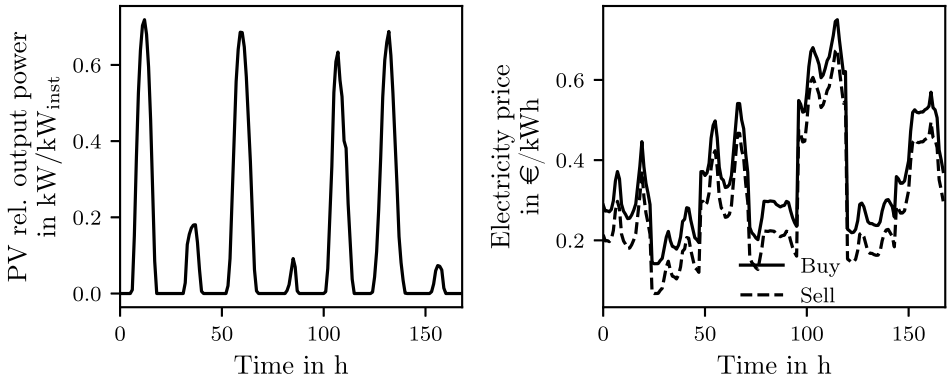

Fig. D.3. Presentation of the time series input data of the relative PV output power and electricity prices of the year 2022. The values shown are based on a time series aggregation with 7 typical days and 24 time steps of 1 h in each case.

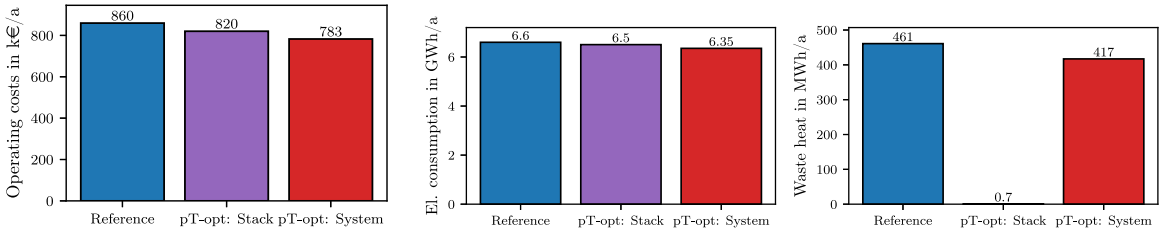

Fig. D.4. Comparison of the annual operating costs for the energy system under consideration, the annual electricity consumption and the annual waste heat of the PEM electrolysis system for the reference case (blue) and the pressure and temperature-optimized case (pT-opt), split into system- (red) and stack-optimized (purple) operation for the year 2022.

to represent a high price level (Appendix D.2.1) and a comparatively low price level (Appendix D.2.2). To align the PV generation with the electricity prices, corresponding weather data is used for the analysis.

D.2.1. High electricity prices

The input data for the high-price scenario is presented in Fig. D.3, with operating parameters over time shown in Fig. D.5 and the resulting costs and electricity demand illustrated in Fig. D.4.

Due to variations in PV output and electricity price profiles, the hydrogen generation profile differs compared to Fig. 8, though similar trends are observed: hydrogen is produced when electricity prices are low or when ample PV power is available. A similar pattern is reflected in the selection of operating parameters. The reference mode generally operates at higher current densities than the optimized modes, with the stack-optimized mode selecting the lowest current densities. The same trend is seen for operating temperature and pressure, where both parameters are also minimized in stack-optimized mode. Notably, although maximum temperatures are selected at several points in time in both optimized modes, this does not occur continuously.

Regarding costs and energy consumption, stack- and system-optimized operations result in reductions of 4.7 % and 9.0 % in operating costs and 1.5 % and 3.8 % in power consumption for the PEM

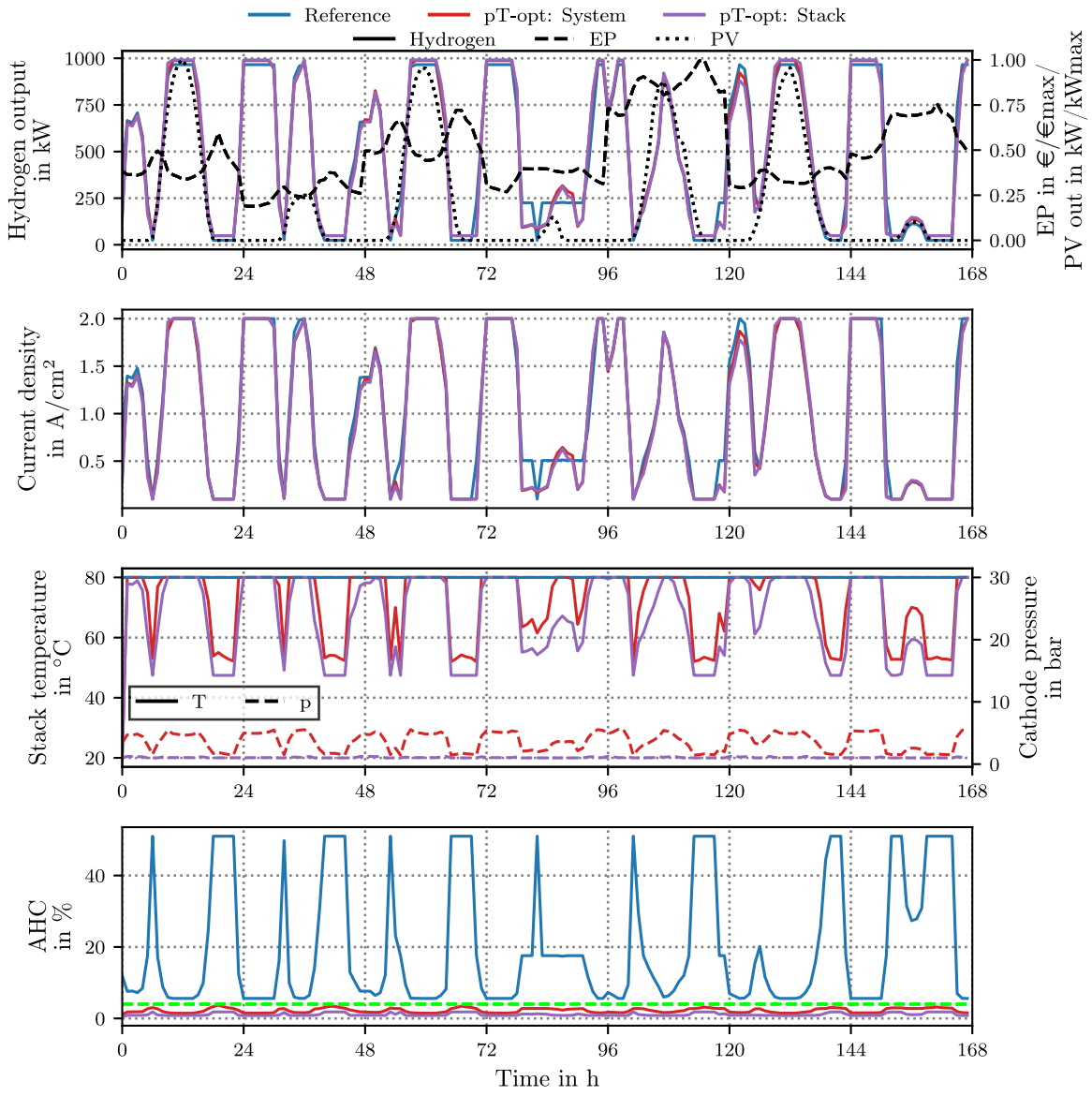

Fig. D.5. Temporal progression of selected operating parameters for the reference case (blue) and the pressure- and temperature-optimized case (pT-opt), split into system- (red) and stack-optimized (purple) operation for an aggregated week of the year 2022 within an energy system. The electricity price and PV output are normalized to their maximum value over the time horizon. The green dotted line indicates the safety limit of the AHC (EP: Electricity price, PV: Photovoltaic, AHC: Anodic hydrogen content).

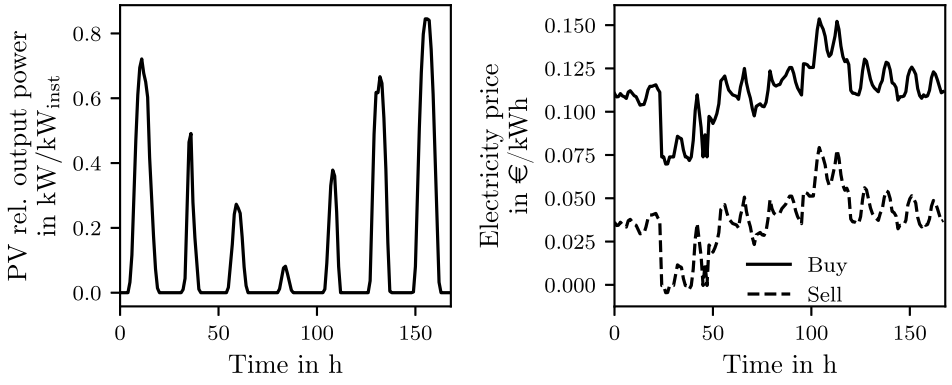

Fig. D.6. Presentation of the time series input data of the relative PV output power and electricity prices of the year 2019. The values shown are based on a time series aggregation with 7 typical days and 24 time steps of 1 h in each case.

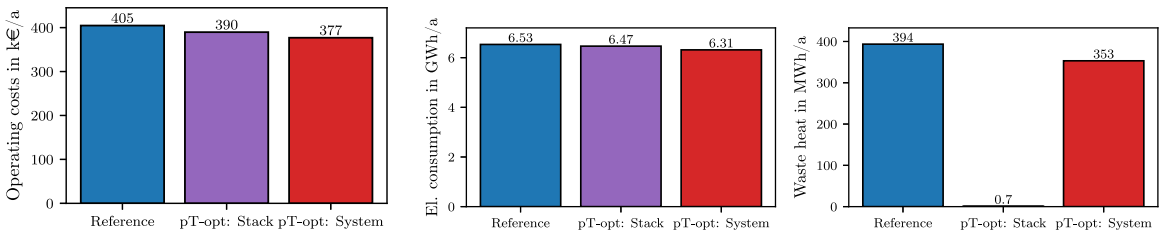

Fig. D.7. Comparison of the annual operating costs for the energy system under consideration, the annual electricity consumption and the annual waste heat of the PEM electrolysis system for the reference case (blue) and the pressure and temperature-optimized case (*pT*-opt), split into system- (red) and stack-optimized (purple) operation for the year 2019.

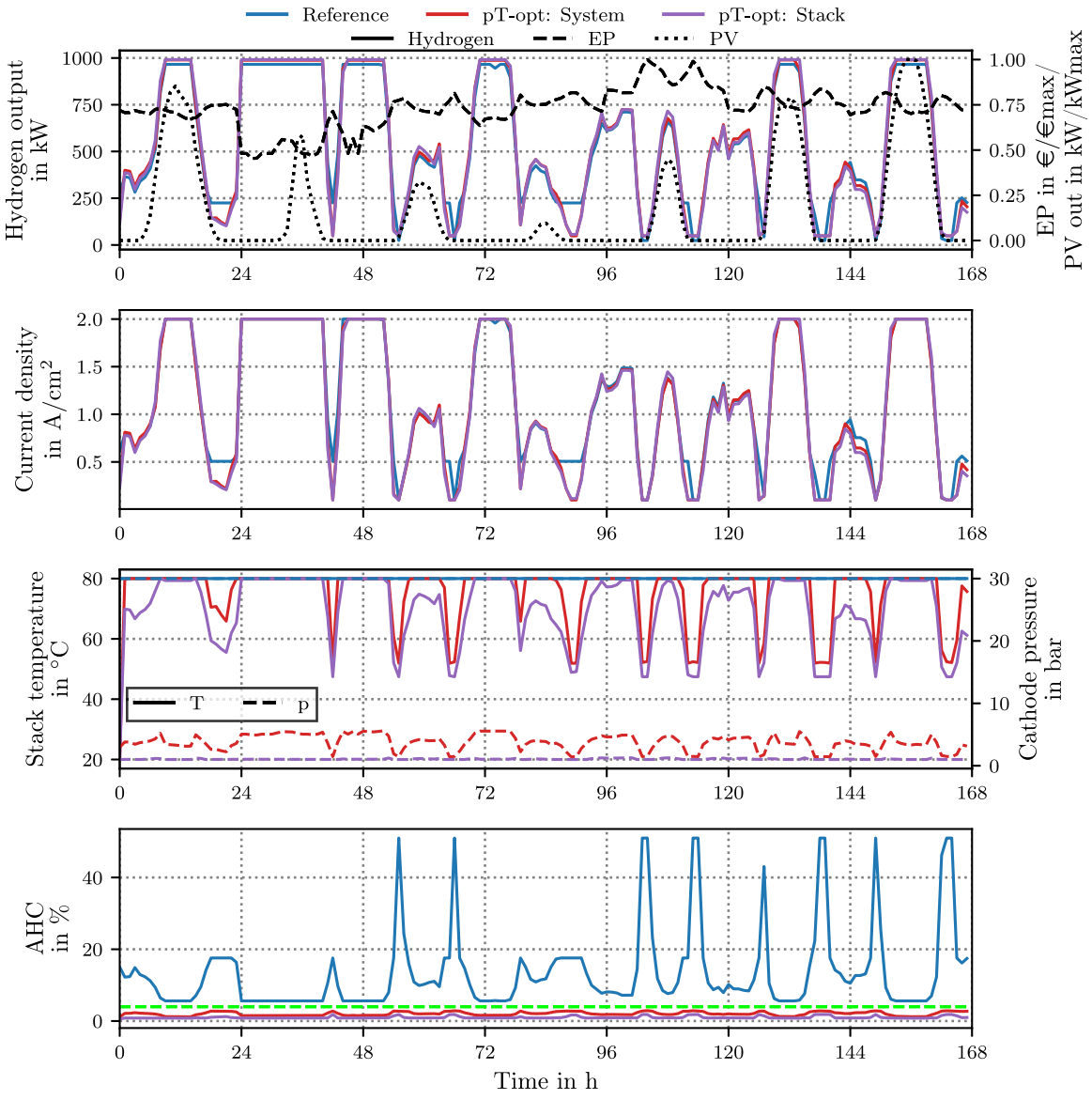

Fig. D.8. Temporal progression of selected operating parameters for the reference case (blue) and the pressure- and temperature-optimized case (*pT*-opt), split into system- (red) and stack-optimized (purple) operation for an aggregated week of the year 2019 within an energy system. The electricity price and PV output are normalized to their maximum value over the time horizon. The green dotted line indicates the safety limit of the AHC (EP: Electricity price, PV: Photovoltaic, AHC: Anodic hydrogen content).

electrolysis system. Additionally, minimal waste heat is generated in stack-optimized operation.

D.2.2. Low electricity prices

The input data for the low-price scenario is presented in Fig. D.6, with operating parameters over time shown in Fig. D.8 and the resulting costs and electricity demand illustrated in Fig. D.7.

While the hydrogen production profile differs due to the adjusted input data, the overall trends remain consistent. The current density follows a similar pattern across all cases, though deviations occur at certain times for reasons previously discussed, with stack-optimized operation consistently maintaining the lowest average current density. However, compared to the high-price scenario, all modes tend to operate more frequently at high current densities, where efficiency gains

are less pronounced compared to the reference case. The selection of operating temperature and pressure aligns with the findings discussed in Appendix D.2.1 and Section 3.2.1, showing fluctuating operation, particularly for temperature, as the electrolyzer is not continuously operated at maximum temperature.

In terms of costs and power consumption, stack- and system-optimized operation reduce operating costs by 3.7 % and 6.9 %, respectively, and reduce the PEM electrolysis system's power consumption by 0.9 % and 3.3 %, respectively. As in the high-price scenario, almost no waste heat is generated in stack-optimized operation.

D.2.3. Conclusion

In summary, for the temperature- and pressure-optimized operation of the PEM electrolysis system within an energy system, similar qualitative and quantitative results are obtained, even with varying input data. It can be confirmed that adjusting the pressure and temperature according to the load point is beneficial, and continuous operation at maximum parameters is not ideal. However, it is recommended to select the maximum temperature at specific points in time.

The resulting cost and electricity savings are also comparable across scenarios. For instance, in the main section, system-optimized operation demonstrated cost savings of 7.1 % and electricity savings of 3.8 %. In the high- and low-price scenarios, savings were 9.0 % and 3.8 %, and 6.9 % and 3.3 %, respectively. While the different input data lead to quantitatively varying savings potentials, these values remain within a similar range, underscoring the robustness of the key conclusions in this paper.

Data availability

The code of the PEM electrolysis system process model and energy system model as well as the input data used in this work is published at https://doi.org/10.5281/zenodo.13269351 under a MIT license.

Code and Data for Paper: Optimizing Temperature and Pressure in PE M Electrolyzers: A Model-Based Approach to Enhanced Efficiency in I ntegrated Energy Systems (Original data) (Zotero)

References

[1] Hauglustaine D, Paulot F, Collins W, Derwent R, Sand M, Boucher O. Climate benefit of a future hydrogen economy. Commun Earth Environ 2022;3(1):1–14. http://dx.doi.org/10.1038/s43247-022-00626-z.

[2] Buttler A, Spliethoff H. Current status of water electrolysis for energy storage, grid balancing and sector coupling via power-to-gas and power-to-liquids: A review. Renew Sustain Energy Rev 2018;82:2440–54. http://dx.doi.org/10.1016/j.rser.2017.09.003.

[3] Thema M, Bauer F, Sterner M. Power-to-gas: Electrolysis and methanation status review. Renew Sustain Energy Rev 2019;112:775–87. http://dx.doi.org/10.1016/j.rser.2019.06.030.

[4] Furfari S, Clerici A. Green hydrogen: The crucial performance of electrolysers fed by variable and intermittent renewable electricity. Eur Phys J Plus 2021;136(5). http://dx.doi.org/10.1140/epjp/s13360-021-01445-5.

[5] Gutiérrez-Martín F, Guerrero-Hernández I. Balancing the grid loads by large scale integration of hydrogen technologies: The case of the Spanish power system. Int J Hydrog Energy 2012;37(2):1151–61. http://dx.doi.org/10.1016/j.ijhydene.2011.09.116.

[6] Kopp M, Coleman D, Stiller C, Scheffer K, Aichinger J, Scheppat B. Energiepark Mainz: Technical and economic analysis of the worldwide largest power-to-gas plant with PEM electrolysis. Int J Hydrog Energy 2017;42(19):13311–20. http://dx.doi.org/10.1016/j.ijhydene.2016.12.145.

[7] Carmo M, Fritz DL, Mergel J, Stolten D. A comprehensive review on PEM water electrolysis. Int J Hydrog Energy 2013;38(12):4901–34. http://dx.doi.org/10.1016/j.ijhydene.2013.01.151.

[8] Götz M, Lefebvre J, Mörs F, McDaniel Koch A, Graf F, Bajohr S, Reimert R, Kolb T. Renewable power-to-gas: A technological and economic review. Renew Energy 2016;85:1371–90. http://dx.doi.org/10.1016/j.renene.2015.07.066.

[9] Glenk G, Holler P, Reichelstein S. Advances in power-to-gas technologies: Cost and conversion efficiency. 2022, http://dx.doi.org/10.2139/ssrn.4300331, SSRN Electronic Journal.

[10] Baader FJ, Bardow A, Dahmen M. MILP formulation for dynamic demand response of electrolyzers. In: 14th international symposium on process systems engineering. Computer aided chemical engineering, Elsevier; 2022, p. 391–6. http://dx.doi.org/10.1016/B978-0-323-85159-6.50065-8.

[11] Scheepers F, Stähler M, Stähler A, Müller M, Lehnert W. Cost-optimized design point and operating strategy of polymer electrolyte membrane electrolyzers. Int J Hydrog Energy 2023;48(33):12185–99. http://dx.doi.org/10.1016/j.ijhydene.2022.11.288.

[12] Schalenbach M, Tjarks G, Carmo M, Lueke W, Mueller M, Stolten D. Acidic or alkaline? Towards a new perspective on the efficiency of water electrolysis. J Electrochem Soc 2016;163(11):3197–208. http://dx.doi.org/10.1149/2.0271611jes.

[13] Scheepers F, Stähler M, Stähler A, Rauls E, Müller M, Carmo M, et al. Temperature optimization for improving polymer electrolyte membrane-water electrolysis system efficiency. Appl Energy 2021;283:116270. http://dx.doi.org/10.1016/j.apenergy.2020.116270.

[14] Grigoriev SA, Fateev VN, Bessarabov DG, Millet P. Current status, research trends, and challenges in water electrolysis science and technology. Int J Hydrog Energy 2020;45(49):26036–58. http://dx.doi.org/10.1016/j.ijhydene.2020.03.109.

[15] Bonanno M, Müller K, Bensmann B, Hanke-Rauschenbach R, Aili D, Franken T, et al. Review and prospects of PEM water electrolysis at elevated temperature operation. Adv Mater Technol 2024;9(2). http://dx.doi.org/10.1002/admt.202300281.

[16] Hancke R, Bujlo P, Holm T, Ulleberg Ø. High-pressure PEM water electrolyser performance up to 180 bar differential pressure. J Power Sources 2024;601:234271. http://dx.doi.org/10.1016/j.jpowsour.2024.234271.

[17] Scheepers F, Stähler M, Stähler A, Rauls E, Müller M, Carmo M, et al. Improving the efficiency of PEM electrolyzers through membrane-specific pressure optimization. Energies 2020;13(3):612. http://dx.doi.org/10.3390/en13030612.

[18] Tjarks G, Gibelhaus A, Lanzerath F, Müller M, Bardow A, Stolten D. Energetically-optimal PEM electrolyzer pressure in power-to-gas plants. Appl Energy 2018;218:192–8. http://dx.doi.org/10.1016/j.apenergy.2018.02.155.

[19] Briguglio N, Brunaccini G, Siracusano S, Randazzo N, Dispenza G, Ferraro M, et al. Design and testing of a compact PEM electrolyzer system. Int J Hydrog Energy 2013;38(26):11519–29. http://dx.doi.org/10.1016/j.ijhydene.2013.04.091.

[20] Kotzur L, Nolting L, Hoffmann M, Groß T, Smolenko A, Priesmann J, et al. A modeler's guide to handle complexity in energy systems optimization. Adv Appl Energy 2021;4:100063. http://dx.doi.org/10.1016/j.adapen.2021.100063.

[21] Wang Y, Bornemann L, Reinert C, Assen N. A method to bridge energy and process system optimization: identifying the feasible operating space for a methanation process in power-to-gas energy systems. Comput Chem Eng 2024;182:108582. http://dx.doi.org/10.1016/j.compchemeng.2023.108582.

[22] Zhang X, Zhang Y. Environment-friendly and economical scheduling optimization for integrated energy system considering power-to-gas technology and carbon capture power plant. J Clean Prod 2020;276:123348. http://dx.doi.org/10.1016/j.jclepro.2020.123348.

[23] Bongartz D, Mitsos A. Deterministic global flowsheet optimization: Between equation-oriented and sequential-modular methods. AIChE J 2019;65(3):1022–34. http://dx.doi.org/10.1002/aic.16507.

[24] Gabrielli P, Flamm B, Eichler A, Gazzani M, Lygeros J, Mazzotti M. Modeling for optimal operation of PEM fuel cells and electrolyzers. In: 2016 IEEE 16th international conference on environment and electrical engineering. IEEE; 2016, p. 1–7. http://dx.doi.org/10.1109/EEEIC.2016.7555707.

[25] Gabrielli P, Gazzani M, Mazzotti M. Electrochemical conversion technologies for optimal design of decentralized multi-energy systems: Modeling framework and technology assessment. Appl Energy 2018;221:557–75. http://dx.doi.org/10.1016/j.apenergy.2018.03.149.

[26] Li J, Lin J, Song Y, Xing X, Fu C. Operation optimization of power to hydrogen and heat (P2HH) in ADN coordinated with the district heating network. IEEE Trans Sustain Energy 2019;10(4):1672–83. http://dx.doi.org/10.1109/TSTE.2018.2868827.

[27] Valverde L, Rosa F, Del Real AJ, Arce A, Bordons C. Modeling, simulation and experimental set-up of a renewable hydrogen-based domestic microgrid. Int J Hydrog Energy 2013;38(27):11672–84. http://dx.doi.org/10.1016/j.ijhydene.2013.06.113.

[28] Prokopou GI, Mödden ML, Mitsos A, Bongartz D. Optimal sizing and operation of electrochemical hydrogen compression. Chem Eng Sci 2024;293:120031. http://dx.doi.org/10.1016/j.ces.2024.120031.

[29] Wiegner JF, Grimm A, Weimann L, Gazzani M. Optimal design and operation of solid sorbent direct air capture processes at varying ambient conditions. Ind Eng Chem Res 2022;61(34):12649–67. http://dx.doi.org/10.1021/acs.iecr.2c00681.

[30] Lee A, Ghouse JH, Eslick JC, Laird CD, Siirola JD, Zamarripa MA, et al. The IDAES process modeling framework and model library—flexibility for process simulation and optimization. J Adv Manuf Process 2021;3(3):10095. http://dx.doi.org/10.1002/amp2.10095.

[31] Nishida N, Stephanopoulos G, Westerberg AW. A review of process synthesis. AIChE J 1981;27(3):321–51. http://dx.doi.org/10.1002/aic.690270302.

[32] Schalenbach M, Hoefner T, Paciok P, Carmo M, Lueke W, Stolten D. Gas permeation through nafion. part 1: Measurements. J Phys Chem C 2015;119(45):25145–55. http://dx.doi.org/10.1021/acs.jpcc.5b04155.

[33] Schalenbach M, Carmo M, Fritz DL, Mergel J, Stolten D. Pressurized PEM water electrolysis: Efficiency and gas crossover. Int J Hydrog Energy 2013;38(35):14921–33. http://dx.doi.org/10.1016/j.ijhydene.2013.09.013.
[34] Klose C, Trinke P, Böhm T, Bensmann B, Vierrath S, Hanke-Rauschenbach R, et al. Membrane interlayer with Pt recombination particles for reduction of the anodic hydrogen content in PEM water electrolysis. J Electrochem Soc 2018;165(16):F1271. http://dx.doi.org/10.1149/2.1241814jes.
[35] Barthelemy H, Weber M, Barbier F. Hydrogen storage: Recent improvements and industrial perspectives. Int J Hydrog Energy 2017;42(11):7254–62. http://dx.doi.org/10.1016/j.ijhydene.2016.03.178.
[36] Muhammed NS, Haq B, Al Shehri D, Al-Ahmed A, Rahman MM, Zaman E. A review on underground hydrogen storage: Insight into geological sites, influencing factors and future outlook. Energy Rep 2022;8:461–99. http://dx.doi.org/10.1016/j.egyr.2021.12.002.
[37] Falcão DS, Pinto A. A review on PEM electrolyzer modelling: Guidelines for beginners. J Clean Prod 2020;261:121184. http://dx.doi.org/10.1016/j.jclepro.2020.121184.
[38] Marangio F, Santarelli M, Calì M. Theoretical model and experimental analysis of a high pressure PEM water electrolyser for hydrogen production. Int J Hydrog Energy 2009;34(3):1143–58. http://dx.doi.org/10.1016/j.ijhydene.2008.11.083.
[39] Mauritz KA, Moore RB. State of understanding of nafion. Chem Rev 2004;104(10):4535–86. http://dx.doi.org/10.1021/cr0207123.
[40] Wächter A, Biegler LT. On the implementation of an interior-point filter line-search algorithm for large-scale nonlinear programming. Math Program 2006;106(1):25–57. http://dx.doi.org/10.1007/s10107-004-0559-y.
[41] Pfenninger S, Staffell I. Long-term patterns of European PV output using 30 years of validated hourly reanalysis and satellite data. Energy 2016;114:1251–65. http://dx.doi.org/10.1016/j.energy.2016.08.060.
[42] Bundesnetzagentur | SMARDde. Market data. 2024.
[43] Eurostat, the Statistical Office of the European Union. Electricity prices for non-household consumers - bi-annual data (from 2007 onwards). 2024.
[44] Bogdanov D, Oyewo AS, Breyer C. Hierarchical approach to energy system modelling: Complexity reduction with minor changes in results. Energy 2023;273:127213. http://dx.doi.org/10.1016/j.energy.2023.127213.
[45] Ward JH. Hierarchical grouping to optimize an objective function. J Amer Statist Assoc 1963;58(301):236–44. http://dx.doi.org/10.1080/01621459.1963.10500845.
[46] Hoffmann M, Kotzur L, Stolten D. The Pareto-optimal temporal aggregation of energy system models. Appl Energy 2022;315:119029. http://dx.doi.org/10.1016/j.apenergy.2022.119029.
[47] Sens L, Piguel Y, Neuling U, Timmerberg S, Wilbrand K, Kaltschmitt M. Cost minimized hydrogen from solar and wind – Production and supply in the European catchment area. Energy Convers Manage 2022;265:115742. http://dx.doi.org/10.1016/j.enconman.2022.115742.
[48] Kotzur L, Markewitz P, Robinius M, Stolten D. Time series aggregation for energy system design: Modeling seasonal storage. Appl Energy 2018;213:123–35. http://dx.doi.org/10.1016/j.apenergy.2018.01.023.
[49] Bynum ML, Hackebeil GA, Hart WE, Laird CD, Nicholson BL, Siirola JD, et al. 3rd ed. Pyomo-optimization modeling in python, vol. 67, Springer Science & Business Media; 2021.
[50] Hart WE, Watson J-P, Woodruff DL. Pyomo: Modeling and solving mathematical programs in Python. Math Program Comput 2011;3(3):219260. http://dx.doi.org/10.1007/s12532-011-0026-8.
[51] Abdelghany MB, Al-Durra A, Zeineldin HH, Gao F. A coordinated multitimescale model predictive control for output power smoothing in hybrid microgrid incorporating hydrogen energy storage. IEEE Trans Ind Inf 2024;20(9):10987–1001. http://dx.doi.org/10.1109/TII.2024.3396343.
[52] Ito H, Miyazaki N, Ishida M, Nakano A. Cross-permeation and consumption of hydrogen during proton exchange membrane electrolysis. Int J Hydrog Energy 2016;41(45):20439–46. http://dx.doi.org/10.1016/j.ijhydene.2016.08.119.
[53] Sayed-Ahmed H, Toldy Á, Santasalo-Aarnio A. Dynamic operation of proton exchange membrane electrolyzers—Critical review. Renew Sustain Energy Rev 2024;189:113883. http://dx.doi.org/10.1016/j.rser.2023.113883.
[54] Di Blasi A, Andaloro L, Siracusano S, Briguglio N, Brunaccini G, Stassi A, et al. Evaluation of materials and components degradation of a PEM electrolyzer for marine applications. Int J Hydrog Energy 2013;38(18):7612–5. http://dx.doi.org/10.1016/j.ijhydene.2012.10.062.
[55] Chandesris M, Médeau V, Guillet N, Chelghoum S, Thoby D, Fouda-Onana F. Membrane degradation in PEM water electrolyzer: Numerical modeling and experimental evidence of the influence of temperature and current density. Int J Hydrog Energy 2015;40(3):1353–66. http://dx.doi.org/10.1016/j.ijhydene.2014.11.111.
[56] Martinez Lopez V, Ziar H, Haverkort J, Zeman M, Isabella O. Dynamic operation of water electrolyzers: A review for applications in photovoltaic systems integration. Renew Sustain Energy Rev 2023;182:113407. http://dx.doi.org/10.1016/j.rser.2023.113407.
[57] Rauls E, Hehemann M, Scheepers F, Müller M, Peters R, Stolten D. System dynamics of polymer electrolyte membrane water electrolyzers and impact of renewable energy sources on systems design. Int J Hydrog Energy 2024;65:83–94. http://dx.doi.org/10.1016/j.ijhydene.2024.03.302.
[58] Moustafa AM, Abdelghany MB, Younis A-SA, Moness M, Al-Durra A, Guerrero JM. Software-defined control of an emulated hydrogen energy storage for energy internet ecosystems. Int J Hydrog Energy 2024;50:893–909. http://dx.doi.org/10.1016/j.ijhydene.2023.08.208.
[59] Linstrom P. NIST chemistry WebBook, NIST standard reference database 69. National Institute of Standards and Technology; 1997, http://dx.doi.org/10.18434/T4D303.
[60] Poling BE, Prausnitz JM, O'Connell JP. The properties of gases and liquids. 5th ed. New York: McGraw-Hill; 2001.
[61] Perry RH, Green DW. Perry 's chemischen-Ingenieure 'Handbuch 7. Edition von Perry, Robert H.; Grün, Don W. veröffentlicht von mcgraw-hill Professionelle Hardcover. 7th ed. New York, NY: McGraw-Hill Professional; 1997.
[62] Burgard A, Eason J, Eslick J, Ghouse J, Lee A, Biegler L, et al. A smooth, square flash formulation for equation-oriented flowsheet optimization. In: Computer aided chemical engineering. 2018, p. 871–6. http://dx.doi.org/10.1016/B978-0-444-64241-7.50140-3.
[63] Reddi K, Elgowainy A, Rustagi N, Gupta E. Two-tier pressure consolidation operation method for hydrogen refueling station cost reduction. Int J Hydrog Energy 2018;43(5):2919–29. http://dx.doi.org/10.1016/j.ijhydene.2017.12.125.